Inorg. Chem. **2006**, *45*, 2925–2941

Dinuclear Copper(II) Complexes with $\{Cu_2(\mu\text{-hydroxo})bis(\mu\text{-carboxylato})\}^+$ Cores and Their Reactions with Sugar Phosphate Esters: A Substrate Binding Model of Fructose-1,6-bisphosphatase

Merii Kato,[†] Tomoaki Tanase,*[,†] and Masahiro Mikuriya[‡]

Department of Chemistry, Faculty of Science, Nara Women's University, Kitauoya-higashi-machi, Nara 630-8285, Japan, and Department of Chemistry, School of Science and Technology, Kwansei Gakuin University, 2-1 Gakuen, Sanda-shi, Hyogo 669-1337, Japan

Received November 10, 2005

Reactions of $CuX_2 \cdot nH_2O$ with the biscarboxylate ligand XDK (H_2XDK = *m*-xylenediamine bis(Kemp's triacid imide)) in the presence of N-donor auxiliary ligands yielded a series of dicopper(II) complexes, $[Cu_2(\mu\text{-OH})(XDK)(L)_2]X$ (L = *N*,*N*,*N*′,*N*′-tetramethylethylenediamine (tetmen), X = NO_3 (**1a**), Cl (**1b**); L = *N*,*N*,*N*′-trimethylethylenediamine (tmen), X = NO_3 (**2a**), Cl (**2b**); L =2,2′-bipyridine (bpy), X = NO_3 (**3**); L = 1,10-phenanthroline (phen), X = NO_3 (**4**); L = 4,4′-dimethyl-2,2′-bipyridine (Me_2bpy), X = NO_3 (**5**); L = 4-methyl-1,10-phenanthroline (Mephen), X = NO_3 (**6**)). Complexes **1**–**6** were characterized by X-ray crystallography (Cu···Cu = 3.1624(6)–3.2910(4) Å), and the electrochemical and magnetic properties were also examined. Complexes **3** and **4** readily reacted with diphenyl phosphoric acid (HDPP) or bis(4-nitrophenyl) phosphoric acid (HBNPP) to give $[Cu_2(\mu\text{-phosphate})(XDK)(L)_2]NO_3$ (L = bpy, phosphate = DPP (**11**); L = phen, phosphate = DPP (**12**), BNPP (**13**)), where the phsophate diester bridges the two copper ions in a μ-1,3-O,O′ bidentate fashion (Cu···Cu = 4.268(3)–4.315(1) Å). Complexes **4** and **6** with phen and Mephen have proven to be good precursors to accommodate a series of sugar monophosphate esters (Sugar-**P**) onto the biscarboxylate-bridged dicopper centers, yielding $[Cu_2(\mu\text{-Sugar-}\mathbf{P})(XDK)(L)_2]$ (Sugar-**P** = α-D-Glc-1-**P** (**23a** and **b**), D-Glc-6-**P** (**24a** and **b**), D-Man-6-**P** (**25a**), D-Fru-6-**P** (**26a** and **b**); L = phen (**a**), Mephen (**b**)) and $[Cu_2(\mu\text{-Gly-}n\text{-}\mathbf{P})(XDK)(Mephen)_2]$ (Gly-*n*-**P** = glycerol *n*-phosphate; *n* = 2 (**21**), 3 (**22**)), where Glc, Man, and Fru are glucose, mannose, and fructose, respectively. The structure of $[Cu_2(\mu\text{-MNPP})(XDK)(phen)_2(CH_3OH)]$ (**20**) was characterized as a reference compound (H_2MNPP = 4-nitrophenyl phosphoric acid). Complexes **4** and **6** also reacted with D-fructose 1,6-bisphosphate (D-Fru-1,6-$\mathbf{P}_2$) to afford the tetranuclear copper(II) complexes formulated as $[Cu_4(\mu\text{-D-Fru-1,6-}\mathbf{P}_2)(XDK)_2(L)_4]$ (L = phen (**27a**), Mephen (**27b**)). The detailed structure of **27a** was determined by X-ray crystallography to involve two different tetranuclear complexes with α- and β-anomers of D-Fru-1,6-$\mathbf{P}_2$, $[Cu_4(\mu\text{-}\alpha\text{-D-Fru-1,6-}\mathbf{P}_2)(XDK)_2(phen)_4]$ and $[Cu_4(\mu\text{-}\beta\text{-D-Fru-1,6-}\mathbf{P}_2)(XDK)_2(phen)_4]$, in which the D-Fru-1,6-$\mathbf{P}_2$ tetravalent anion bridges the two $[Cu_2(XDK)(phen)_2]^{2+}$ units through the C1 and C6 phosphate groups in a μ-1,3-O,O′ bidentate fashion (Cu···Cu = 4.042(2)–4.100(2) Å). Notably, the structure with α-D-Fru-1,6-$\mathbf{P}_2$ demonstrated the presence of a strong hydrogen bond between the C2 hydroxyl group and the C1 phosphate oxygen atom, which may support the previously proposed catalytic mechanism in the active site of fructose-1,6-bisphosphatase.

Introduction

Recent biological studies have revealed that carboxylate-bridged dinuclear metal units are involved in a number of metalloproteins as a ubiquitous bioinorganic motif.[1,2] In the active sites of non-heme diiron proteins, hemerythrin (Hr), ribonucleotide reductase (RR), and methane monooxygenase (MMO), the redox-active diiron centers are bridged by carboxylate groups of the amino acid side-chains and function coupled with molecular-oxygen-metabolizing processes.[1] A wide variety of synthetic model complexes have

* To whom correspondence should be addressed. E-mail: tanase@cc.nara-wu.ac.jp.
[†] Nara Women's University.
[‡] Kwansei Gakuin University.

10.1021/ic051942d CCC: $33.50
Published on Web 03/02/2006

been prepared to mimic their structures and functions.[1] It has also been elucidated that carboxylate-bridged divalent dimetal ions, such as Mg^{2+}, Mn^{2+}, Co^{2+}, Ni^{2+}, and Zn^{2+}, are involved in many nonredox-active enzymatic processes, including biological transfer reactions of phosphoryl, acyl, and other carbonyl groups promoted by phosphatases, nucleases, amidases, peptidases, etc.[2,3] For the metalloenzymes that promote phosphoryl group transfer reactions, a cooperative two-metal activation mechanism has prevalently been accepted on the basis of the crystal structures for the 3′,5′-exonuclease of DNA polymerase I.[3] A substrate phosphate ester is bound to the two metal ions in an asymmetric monodentate fashion and activated toward in-line attack by a nucleophile that is generated at an appropriate open site of one metal center. The modified two-metal-ion mechanism with a bidentate phosphate bridge has also been proposed in regard to the X-ray structures of other phosphatases.[2e]

Among phosphate-containing metabolites, sugar phosphate esters are known to play crucial roles as intermediate compounds in regulating and maintaining the bioenergetic systems,[4] and Lewis acidic divalent metal ions, such as Mg^{2+}, Ca^{2+}, Mn^{2+}, Fe^{2+}, Co^{2+}, and Zn^{2+},[5−9] are frequently required for the metalloenzymes that promote transformations of sugar phosphate esters. In particular, fructose-1,6-bisphosphatase (Fru-1,6-Pase) involves biscarboxylate-bridged dimetal ions (Mn^{2+}, Zn^{2+}, Mg^{2+}) and promotes the hydrolysis of α-D-fructose 1,6-bisphosphate to produce D-fructose 6-phosphate.[5] Despite the importance of elucidating interactions between sugar phosphates and metal ions, much less attention has been devoted to the bioinorganic chemistry with sugar phosphate esters, and characterized metal complexes containing free sugar phosphate esters have extremely been scarce. Recently, we have reported the tetranuclear copper(II) complexes of α-D-glucose-1-phosphate (α-D-Glc-1-**P**), $[Cu_4(\mu\text{-OH})(\mu_4\text{-}\alpha\text{-D-Glc-1-}\mathbf{P})_2(L)_4(H_2O)_2](NO_3)_3$ (L = bpy, phen), and $[Cu_4(\mu_4\text{-}\alpha\text{-D-Glc-1-}\mathbf{P})_2(\mu\text{-}CH_3COO)_2(bpy)_4](NO_3)_2$, in which the α-D-Glc-1-**P** dianion connects four copper(II) ions in bidentate 1,3-η^1,η^1-O,O′ and monodentate η^1,η^1-O″ bridging modes.[10] Although several structures for sodium, potassium, and barium salts of some sugar phosphate esters, including D-glucose *n*-phosphate (*n* = 1, 6), D-fructose *n*-phosphate (*n* = 1, 6), and β-D-fructose 1,6-bisphosphate, have been reported,[11] the tetracopper complexes with α-D-Glc-1-**P** are the first examples of transition-metal complexes containing free sugar phosphate esters. Despite the novelty of the complexes, it is noteworthy that the tetranuclear copper(II) cores did not act as efficient scaffolds binding a series of sugar phosphate esters because of the absence of auxiliary bridging ligands.

In the present study, we have tried to synthesize the biscarboxylate-bridged dicopper(II) complexes containing a series of sugar phosphate esters by utilizing the biscarboxylate ligand XDK (H_2XDK = *m*-xylenediamine bis(Kemp's triacid imide)) and imine-based chelating ligands. The XDK has already proven to be an efficient dinucleating ligand in stabilizing a variety of dinuclear metal centers.[12−14] The present ligand system has led to successful isolation of the dinuclear and the tetranuclear copper(II) complexes with sugar phosphate esters, $[Cu_2(\mu\text{-sugar monophosphate})(XDK)(L)_2]$ and $[Cu_4(\mu\text{-D-fructose 1,6-bisphosphate})(XDK)_2(L)_4]$, where L = phen and 4-methyl phen. In particular, the latter tetracopper(II) complex was characterized by X-ray crystallography and could provide useful insights into the substrate binding and activation of Fru-1,6-Pase.

Experimental Section

Materials. All reagents were of the best commercial grade and were used as received. *m*-Xylenediamine bis(Kemp's triacid imide)

(1) (a) Lippard, S. J.; Berg, J. M. *Principles of Bioinorganic Chemistry*; University Science Books: Mill Valley, CA, 1994. (b) Feig, A. L.; Lippard, S. J. *Chem. Rev.* **1994**, *94*, 759. (c) Tshuva, E. Y.; Lippard, S. J. *Chem. Rev.* **2004**, *104*, 987 and references therein.

(2) (a) Vallee, B. L.; Auld, D. S. *Biochemistry* **1993**, *32*, 6493. (b) Fenton, D. E.; Okawa, H. *J. Chem. Soc., Dalton Trans.* **1993**, 1349. (c) Wilcox, D. E. *Chem. Rev.* **1996**, *96*, 2435. (d) Cowan, J. A. *Chem. Rev.* **1998**, *98*, 1067. (e) Strater, N.; Lipscomb, W. N.; Klabunde, T.; Krebs, B. *Angew. Chem., Int. Ed. Engl.* **1996**, *35*, 2024.

(3) (a) Beese, L. S.; Steitz, T. A. *EMBO J.* **1991**, *10*, 25. (b) Steitz, T. A.; Smerdon, S. J.; Jager, J.; Joyce, C. M. *Science* **1994**, *266*, 2022. (c) Steitz, T. A.; Steitz, J. *Proc. Natl. Acad. Sci., U.S.A.* **1993**, *90*, 6498.

(4) (a) Voet, D.; Voet, J. G. *Biochemistry*; John Wiley & Sons: New York, 1995; pp 443−512. (b) He, X.; Agnihotri, G.; Liu, H.-W. *Chem. Rev.* **2000**, *100*, 4615. (c) Sears, P.; Wong, C.-H. *Angew. Chem. Int. Ed.* **1999**, *38*, 2300.

(5) (a) Zhang, Y.; Liang, J.-Y.; Huang, S.; Ke, H.; Lipscomb, W. N. *Biochemistry* **1993**, *32*, 1844. (b) Xue, Y.; Huang, S.; Liang, J.-Y.; Zhang, Y.; Lipscomb, W. N. *Proc. Natl. Acad. Sci. U.S.A.* **1994**, *91*, 12482. (c) Villeret, V.; Huang, S.; Zhang, Y.; Lipscomb, W. N. *Biochemistry* **1995**, *34*, 4307. (d) Bone, R.; Frank, L.; Springer, J. P.; Atack, J. R. *Biochemistry* **1994**, *33*, 9468.

(6) (a) Cleasby, A.; Wonacott, A.; Skarzynski, T.; Hubbard, R. E.; Davies, G. J.; Proudfoot, A. E. I.; Bernard, A. R.; Payton, M. A.; Wells, T. N. C. *Nature Struct. Biol.* **1996**, *3*, 470. (b) Wells, T. N. C.; Coulin, F.; Payton, M. A.; Proudfoot, A. E. I. *Biochemistry*, **1993**, *32*, 1294.

(7) (a) Swan, M. K.; Solomons, J. T. G.; Beeson, C. C.; Hansen, T.; Schonheit, P.; Davies, C. *J. Biol. Chem.* **2003**, *278*, 47261. (b) Berrisford, J. M.; Akerboom, J.; Turnbull, A. P.; de Geus, D.; Sedelnikova, S. E.; Staton, I.; McLeod, C. W.; Verhees, C. H.; van der Oost, J.; Rice, D. W.; Baker, P. J. *J. Biol. Chem.* **2003**, *278*, 33290.

(8) Lahiri, S. D.; Zhang, G.; Dunaway-Mariano, D.; Allen, K. N. *Science* **2003**, *299*, 2067.

(9) (a) Andersson, I.; Knight, S.; Schneider, G.; Lindqvist, Y.; Lundqvist, T.; Branden, C.-I.; Lorimer, G. H. *Nature* **1989**, *337*, 229. (b) Mizohata, E.; Matsumura, H.; Okano, Y.; Kumei, M.; Takuma, H.; Onodera, J.; Kato, K.; Shibata, N.; Inoue, T.; Yokota, A.; Kai, Y. *J. Mol. Biol.* **2002**, *316*, 679. (c) Karkehabadi, S.; Taylor, T. C.; Andersson, I. *J. Mol. Biol.* **2003**, *334*, 65.

(10) Kato, M.; Tanase, T. *Inorg. Chem.* **2005**, *44*, 8.

(11) For example, see: (a) Narendra, N.; Seshadri, T. P.; Viswamitra, M. A. *Acta Crystallogr. C* **1984**, *40*, 1338. (b) Lis, T. *Carbohydr. Res.* **1985**, *135*, 187. (c) Narendra, N.; Seshadri, T. P.; Viswamitra, M. A. *Acta Crystallogr. C* **1985**, *41*, 31. (d) Narendra, N.; Seshadri, T. P.; Viswamitra, M. A. *Acta Crystallogr. C* **1985**, *41*, 1612.

(12) (a) Goldberg, D. P.; Watton, S. P.; Masschelein, A.; Wimmer, L.; Lippard, S. J. *J. Am. Chem. Soc.* **1993**, *115*, 5346. (b) Watton, S. P.; Masschelein, A.; Rebek, J., Jr.; Lippard, S. J. *J. Am. Chem. Soc.* **1994**, *116*, 5196. (c) Tanase, T.; Watton, S. P.; Lippard, S. J. *J. Am. Chem. Soc.* **1994**, *116*, 9401. (d) Yun, J. W.; Tanase, T.; Pence, L. E.; Lippard, S. J. *J. Am. Chem. Soc.* **1995**, *117*, 4407. (e) Tanase, T.; Yun, J. W.; Lippard, S. J. *Inorg. Chem.* **1995**, *34*, 4220. (f) Tanase, T.; Lippard, S. J. *Inorg. Chem.* **1995**, *34*, 4682. (g) Tanase, T.; Yun, J. W.; Lippard, S. J. *Inorg. Chem.* **1996**, *35*, 3585. (h) Yun, J. W.; Tanase, T.; Lippard, S. J. *Inorg. Chem.* **1996**, *35*, 7590. (i) LeCloux, D. D.; Lippard, S. J. *Inorg. Chem.* **1997**, *36*, 4035. (j) He, C.; Lippard, S. J. *J. Am. Chem. Soc.* **1998**, *120*, 105. (k) Herold, S.; Lippard, S. *J. Am. Chem. Soc.* **1997**, *119*, 145.

(13) Tanase, T.; Inukai, H.; Onaka, T.; Kato, M.; Yano, S.; Lippard, S. J. *Inorg. Chem.* **2001**, *40*, 3943.

(14) (a) Hagen, K. S.; Lachicotte, R.; Kitaygorodskiy, A. *J. Am. Chem. Soc.* **1993**, *115*, 12617. (b) Hagen, K. S.; Lachicotte, R.; Kitaygorodskiy, A.; Elbouadili, A. *Angew. Chem., Int. Ed. Engl.* **1993**, *32*, 1321.

and its sodium salt (H_2XDK and Na_2XDK·$4H_2O$) were prepared by known methods.[12f,15] The following abbreviations are used: tetmen, *N*,*N*,*N*′,*N*′-tetramethylethylenediamine; tmen, *N*,*N*,*N*′-trimethylethylenediamine; bpy, 2,2′-bipyridine; phen, 1,10-phenanthroline; Me_2bpy, 4,4′-dimethyl-2,2′-bipyridine; Mephen, 4-methyl-1,10-phenanthroline; HDPP, diphenyl phosphoric acid; HBNPP, bis(4-nitrophenyl) phosphoric acid; Na_2MNPP, 4-nitrophenyl phosphate disodium salt; Na_2[Gly-2-**P**], glycerol 2-phosphate disodium salt; Na_2[Gly-3-**P**], glycerol 3-phosphate disodium salt; Na_2[α-D-Glc-1-**P**], α-D-glucose 1-phosphate disodium salt; Na_2[D-Glc-6-**P**], D-glucose 6-phosphate disodium salt; Na_2[D-Man-6-**P**], D-mannose 6-phosphate disodium salt; Na_2[D-Fru-6-**P**], D-fructose 6-phosphate disodium salt; Na_n[D-Fru-1,6-$\mathbf{P}_2$], D-fructose 1,6-diphosphate sodium salt.

Measurements. Electronic absorption spectra were recorded on a Shimadzu UV-3100 spectrometer, and circular dichroism spectra were measured on a Jasco J-720 spectropolarimeter. IR spectra were measured on KBr pellets with a Jasco FT/IR 410 spectrometer. Cyclic voltammograms were obtained using a Hokuto Denko HZ-3000 voltammetric analyzer using a conventional three-electrode system; glassy carbon as the working electrode, platinum wire as the counter electrode, and a $Ag/AgPF_6$ reference electrode. Variable-temperature magnetic susceptibility measurements were carried out with a Quantum Design MPMS-5S superconducting quantum interference device (SQUID) susceptometer over a range of 4.5−300 K, and the obtained magnetic susceptibility data were fitted with the modified Bleany−Bowers equation.[16] Electrospray ionization mass spectra were recorded on an Applied Biosystems Mariner spectrometer in positive mode of detection.

Preparation of [Cu_2(μ-OH)(XDK)(L)$_2$]X (L = tetmen, X = NO_3 (1a), Cl (1b); L = tmen, X = NO_3 (2a), Cl (2b)). Na_2XDK·$4H_2O$ (50 mg, 0.072 mmol) was added to a solution of $Cu(NO_3)_2$·$3H_2O$ (33 mg, 0.14 mmol) in methanol (10 mL). The solution was stirred at room temperature for 30 min. A portion of tetmen (0.14 mmol) was added to the solution, which was further stirred for 3 h. The solution was concentrated to dryness, and the residue was extracted with dichloromethane. The extract was passed through a glass filter to remove the inorganic salts and was concentrated to almost dryness. After addition of MeOH (2 mL) and Et_2O (0.5 mL), the solution was allowed to stand at −4 °C to yield pale blue crystals of [Cu_2(μ-OH)(XDK)(tetmen)$_2$]NO_3·$0.5CH_2Cl_2$ (**1a**·$0.5CH_2Cl_2$), which were collected, washed with Et_2O, and dried under vacuum (69 mg, 93% with respect to Cu). Anal. Calcd for $C_{44.5}H_{72}O_{12}N_7ClCu_2$: C, 50.44; H, 6.85; N, 9.25. Found: C, 50.90; H, 6.80; N, 9.51. IR (KBr, cm^{-1}): 1727 (s), 1688 (s), 1589 (s), 1466 (m), 1384 (m, br), 1201 (m). UV−vis (in CH_2Cl_2): λ_{max} (ε) 732 nm (3.18×10^2 M^{-1} cm^{-1}). Mass spectrum (ESI): *m*/*z* 953.454 (M^+, calcd 953.387). Recrystallization of **1a**·$0.5CH_2Cl_2$ from a MeOH/Et_2O mixed solvent at room temperature yielded block-shaped crystals of **1a**·$2CH_3OH$ suitable for X-ray crystallography.

Procedures similar to those described above using $CuCl_2$·$2H_2O$ and tetmen and those using CuX_2·nH_2O (X = NO_3, Cl) and tmen yielded [Cu_2(μ-OH)(XDK)(tetmen)$_2$]Cl·$3H_2O$ (**1b**·$3H_2O$), [Cu_2(μ-OH)(XDK)(tmen)$_2$]NO_3·$2H_2O$ (**2a**·$2H_2O$), and [Cu_2(μ-OH)(XDK)(tmen)$_2$]Cl·$0.5CH_2Cl_2$ (**2b**·$0.5CH_2Cl_2$). For **1b**·$3H_2O$, the yield was 37%. Anal. Calcd for $C_{44}H_{77}O_{12}N_6ClCu_2$: C, 50.59; H, 7.43; N, 8.04. Found: C, 50.28; H, 7.58; N, 8.19. IR (KBr, cm^{-1}): 1727 (s), 1687 (s), 1589 (s), 1466 (m), 1363 (m), 1201 (m). UV−vis (in CH_2Cl_2): λ_{max} (ε) 733 nm (3.27×10^2 M^{-1} cm^{-1}). For **2a**·$2H_2O$, the yield was 58%. Anal. Calcd for $C_{42}H_{71}O_{14}N_7Cu_2$: C, 49.21; H, 6.98; N, 9.56. Found: C, 49.17; H, 7.04; N, 9.68. IR (KBr, cm^{-1}): 1729 (s), 1690 (s), 1594 (s), 1465 (m), 1360 (m, br), 1200 (m). UV−vis (in CH_2Cl_2): λ_{max} (ε) 725 nm (3.16×10^2 M^{-1} cm^{-1}). Mass spectrum (ESI): *m*/*z* 925.431 (M^+, calcd 925.356). For **2b**·$0.5CH_2Cl_2$, the yield was 69%. Anal. Calcd for $C_{42.5}H_{68}O_9N_6Cl_2Cu_2$: C, 50.79; H, 6.82; N, 8.36. Found: C, 50.48; H, 6.58; N, 8.38. IR (KBr, cm^{-1}): 1729 (s), 1689 (s), 1595 (s), 1464 (m), 1360 (m), 1200 (m). UV−vis (in CH_2Cl_2): λ_{max} (ε) 721 nm (3.34×10^2 M^{-1} cm^{-1}). Recrystallization of **1b**·$3H_2O$ and **2a**·$2H_2O$ from a MeOH/Et_2O mixed solvent at room temperature produced block-shaped crystals of **1b**·CH_3OH and **2a**·H_2O suitable for X-ray crystallography.

Preparation of [Cu_2(μ-OH)(XDK)(L)$_2$]NO_3 (L = bpy (3), phen (4), Me_2bpy (5), Mephen, (6)). A portion of Na_2XDK·$4H_2O$ (100 mg, 0.14 mmol) was dissolved in CH_3OH (8 mL), to which $Cu(NO_3)_2$·$3H_2O$ (35 mg, 0.14 mmol) was added. The solution was stirred at room temperature for 30 min, and bpy (0.14 mmol) was added to the solution. The reaction mixture was stirred for another 30 min. The solution was concentrated to dryness, and the residue was extracted with dichloromethane. Addition of MeOH (1 mL) and Et_2O (1 mL) to the concentrated solution (1 mL) afforded blue crystals of [Cu_2(μ-OH)(XDK)(bpy)$_2$]NO_3·CH_2Cl_2 (**3**·CH_2Cl_2) in a 90% yield (74 mg). Anal. Calcd for $C_{53}H_{57}O_{12}N_7Cl_2Cu_2$: C, 53.85; H, 4.86; N, 8.29. Found: C, 53.61; H, 4.72; N, 8.24. IR (KBr, cm^{-1}): 1730 (s), 1685 (s), 1595 (s), 1446 (m), 1358 (m, br), 1194 (m), 765 (m). UV−vis (in CH_2Cl_2): λ_{max} (ε) 724 nm (2.08×10^2 M^{-1} cm^{-1}). Mass spectrum (ESI): *m*/*z* 1033.238 (M^+, calcd 1033.262). Recrystallization of **3**·CH_2Cl_2 from a CH_2Cl_2/MeOH/Et_2O mixed solvent at room temperature gave block-shaped crystals of **3**·$4CH_2Cl_2$ which were suitable for X-ray crystallography.

Procedures similar to those described above, but using phen, Me_2bpy, and Mephen, yielded [Cu_2(μ-OH)(XDK)(phen)$_2$]NO_3·$2CH_2Cl_2$ (**4**·$2CH_2Cl_2$), [Cu_2(μ-OH)(XDK)(Me_2bpy)$_2$]NO_3·H_2O (**5**·H_2O), and [Cu_2(μ-OH)(XDK)(Mephen)$_2$]NO_3·$1.5CH_2Cl_2$·CH_3OH (**6**·$1.5CH_2Cl_2$·CH_3OH), respectively. For **4**·$2CH_2Cl_2$, the yield was 59%. Anal. Calcd for $C_{58}H_{59}O_{12}N_7Cl_4Cu_2$: C, 52.97; H, 4.52; N, 7.46. Found: C, 52.64; H, 4.41; N, 7.93. IR (KBr, cm^{-1}): 1729 (s), 1685 (s), 1598 (s), 1518 (m), 1360 (m, br), 1194 (m). UV−vis (in CH_2Cl_2): λ_{max} (ε) 731 nm (1.93×10^2 M^{-1} cm^{-1}). Mass spectrum (ESI): *m*/*z* 1081.250 (M^+, calcd 1081.262). For **5**·H_2O, the yield was 41%. Anal. Calcd for $C_{56}H_{65}O_{13}N_7Cu_2$: C, 57.43; H, 5.59; N, 8.37. Found: C, 57.40; H, 5.19; N, 8.33. IR (KBr, cm^{-1}): 1728 (s), 1685 (s), 1617 (s), 1595 (m), 1462 (w), 1384 (m, br), 1195 (m). UV−vis (in CH_2Cl_2): λ_{max} (ε) 721 nm (2.15×10^2 M^{-1} cm^{-1}). Mass spectrum (ESI): *m*/*z* 1089.314 (M^+, calcd 1089.324). For **6**·$1.5CH_2Cl_2$·CH_3OH, the yield was 61%. Anal. Calcd for $C_{60.5}H_{66}O_{13}N_7Cl_3Cu_2$: C, 54.53; H, 4.99; N, 7.36. Found: C, 54.48; H, 5.25; N, 7.53. IR (KBr, cm^{-1}): 1727 (s), 1684 (s), 1596 (s), 1384 (s), 1360 (m, br), 1195 (m). UV−vis (in CH_2Cl_2): λ_{max} (ε) 725 nm (1.62×10^2 M^{-1} cm^{-1}). Mass spectrum (ESI): *m*/*z* 1109.313 (M^+, calcd 1109.293). Recrystallization of **4**·$2CH_2Cl_2$, **5**·H_2O, and **6**·$1.5CH_2Cl_2$·CH_3OH from a CH_2Cl_2/MeOH/Et_2O mixed solvent at room temperature gave block-shaped crystals of **4**·$1.5CH_2Cl_2$, **5**·$2CH_2Cl_2$·CH_3OH·H_2O, and **6**·CH_2Cl_2·$2CH_3OH$·$0.5H_2O$, respectively, which were suitable for X-ray crystallography.

Preparation of [Cu_2(μ-η^1,η^1-$(RO)_2PO_2$)(XDK)(L)$_2$]NO_3 (R = Ph, L = bpy (11), phen (12); R = 4-NO_2Ph, L = phen (13)). HDPP (10 mg, 0.040 mmol) was added to a solution of **3**·CH_2Cl_2 (48 mg, 0.041 mmol) in CH_2Cl_2 (5 mL). The reaction mixture was stirred at room temperature for 30 min. The solvent was evaporated under reduced pressure, and the residue was crystallized from a CH_2Cl_2/Et_2O mixed solvent to give blue microcrystals of [Cu_2(μ-

(15) Rebek. J., Jr.; Marshall, L.; Wolak, R.; Parris, K.; Killoran, M.; Askew, B.; Nemeth, D.; Islam, N. *J. Am. Chem. Soc.* **1985**, *107*, 7476.
(16) Bleaney, B.; Bowers, K. D. *Proc. R. Soc. London., Ser. A* **1952**, *214*, 451.

η^1,η^1-DPP)(XDK)(bpy)$_2$]NO_3·CH_2Cl_2 (**11**·CH_2Cl_2) in a 57% yield (33 mg). Anal. Calcd for $C_{65}H_{66}O_{15}N_7Cl_2Cu_2P$: C, 55.20; H, 4.70; N, 6.93. Found: C, 55.48; H, 4.50; N, 6.94. IR (KBr, cm^{-1}): 1728 (s), 1686 (s), 1600 (s), 1447 (m), 1384 (s), 1200 (m, br), 1095 (m), 918 (m, br), 768 (s). UV−vis (in CH_3OH): λ_{max} (ϵ) 719 nm (1.47×10^2) ($M^{-1}cm^{-1}$). Recrystallization of **11**·CH_2Cl_2 from a CH_2Cl_2/MeOH/Et_2O mixed solvent at room temperature gave block-shaped crystals of **11**·$2CH_3OH$·$2.5H_2O$ which were suitable for X-ray crystallography.

Similar reactions of **4**·$2CH_2Cl_2$ with HDPP and HBNPP gave [Cu_2(μ-η^1,η^1-DPP)(XDK)(phen)$_2$]NO_3·CH_2Cl_2 (**12**·CH_2Cl_2) and [Cu_2(μ-η^1,η^1-BNPP)(XDK)(phen)$_2$]NO_3·$3H_2O$ (**13**·$3H_2O$), respectively. For **12**·CH_2Cl_2, the yield was 82%. Anal. Calcd for $C_{69}H_{66}O_{15}N_7Cl_2Cu_2P$: C, 56.68; H, 4.55; N, 6.71. Found: C, 56.50; H, 4.56; N, 6.72. IR (KBr, cm^{-1}): 1729 (s), 1685 (s), 1614 (s), 1594 (w), 1385 (s), 1359 (m), 1198 (m), 1096 (m). UV−vis (in CH_3OH): λ_{max} (ϵ) 735 nm (1.06×10^2 M^{-1} cm^{-1}). For **13**·$3H_2O$, the yield was 43%. Anal. Calcd for $C_{68}H_{68}O_{22}N_9Cu_2P$: C, 53.68; H, 4.51; N, 8.29. Found: C, 53.86; H, 4.36; N, 8.34. IR (KBr, cm^{-1}): 1729 (s), 1686 (s), 1610 (s), 1590 (s), 1520 (s), 1344 (m, br), 1227 (m), 1108 (m, br), 851 (m), 723 (m). UV−vis (in CH_2Cl_2): λ_{max} (ϵ) 732 nm (7.62×10^2 M^{-1} cm^{-1}). Recrystallization of **12**·CH_2Cl_2 and **13**·$3H_2O$ from a CH_2Cl_2/MeOH/Et_2O mixed solvent at room temperature yielded block-shaped crystals of **12**·$2CH_2Cl_2$·$0.5CH_3OH$·$0.5H_2O$ and **13**·$8CH_2Cl_2$, respectively, which were suitable for X-ray crystallography.

Preparation of [Cu_2(μ-η^1,η^1-$(RO)_2PO_2$)$(NO_3)_2(L)_2$] (R = Ph, L = Me$_2$bpy (14); R = 4-NO_2Ph, L = tetmen (15)). HDPP (18 mg, 0.072 mmol) was added to a dichloromethane solution (5 mL) containing **5**·H_2O (66 mg, 0.056 mmol). The reaction mixture was stirred at room temperature for 1h, and the solvent was removed under reduced pressure. The residue was extracted with dichloromethane (2 mL), and Et_2O (0.8 mL) was added to the extract. The resulting solution was allowed to stand at 2 °C to give blue crystals of [Cu_2(μ-η^1,η^1-DPP)$_2(NO_3)_2$(Me$_2$bpy)$_2$]·H_2O (**14**·H_2O) in a 58% yield (37 mg). Anal. Calcd for $C_{48}H_{46}O_{15}N_6Cu_2P_2$: C, 50.75; H, 4.08; N, 7.40. Found: C, 50.98; H, 3.89; N, 7.30. IR (KBr, cm^{-1}): 1492 (s), 1456 (s), 1269 (s), 1208 (s), 1097 (s), 920 (s). UV−vis (in CH_3OH): λ_{max} (ϵ) 702 nm (1.63×10^2 M^{-1} cm^{-1}). A similar procedure using **1a**·$0.5CH_2Cl_2$ (54 mg, 0.051 mmol) and HBNPP (34 mg, 0.10 mmol) gave blue crystals of [Cu_2(μ-η^1,η^1-BNPP)$_2(NO_3)_2$(tetmen)$_2$]·$0.5CH_2Cl_2$ (**15**·$0.5CH_2Cl_2$) in a 29% yield (18 mg). Anal. Calcd for $C_{36.5}H_{49}O_{22}N_{10}ClCu_2P_2$: C, 36.40; H, 4.10; N, 11.63. Found: C, 36.49; H, 4.06; N, 11.35. IR (KBr, cm^{-1}): 1611 (m), 1592 (s), 1527 (s), 1517 (s), 1463 (s), 1342 (s), 1109 (s), 903 (s), 750 (m). UV−vis (in CH_2Cl_2): λ_{max} (ϵ) 723 nm (2.51×10^2 M^{-1} cm^{-1}). Recrystallization of **14**·H_2O and **15**·$0.5CH_2Cl_2$ from a CH_2Cl_2/Et_2O mixed solvent at room temperature produced block-shaped crystals of **14** and **15**, respectively, which were suitable for X-ray crystallography.

Preparation of [Cu_2(μ-MNPP)(XDK)(phen)$_2$(CH_3OH)]·CH_3OH (20·CH_3OH). Na_2MNPP·$6H_2O$ (15 mg, 0.040 mmol) dissolved in a CH_3OH/CH_2Cl_2 (6 mL) mixed solvent was added to a solution of **4**·$2CH_2Cl_2$ (43 mg, 0.033 mmol) in CH_3OH (5 mL). The reaction mixture was stirred at room temperature for 12 h. The solvent was then evaporated under reduced pressure, and the residue was extracted with CH_3OH (6 mL). Addition of Et_2O (0.5 mL) to the concentrated solution yielded block-shaped blue crystals of [Cu_2(μ-MNPP)(XDK)(phen)$_2$(CH_3OH)]·CH_3OH (**20**·CH_3OH; 12 mg, 28%). Anal. Calcd for $C_{64}H_{66}O_{16}N_7Cu_2P$: C, 57.05; H, 4.94; N, 7.28. Found: C, 57.19; H, 4.79; N, 7.45. IR (KBr, cm^{-1}): 1727 (s), 1689 (s), 1619 (s), 1590 (s), 1359 (m), 1338 (s), 1189 (s), 880 (m), 848 (s), 723 (s) cm^{-1}. UV−vis (in CH_2Cl_2): λ_{max} (ϵ) 727 nm (1.05×10^2 M^{-1} cm^{-1}). Recrystallization of **20**·CH_3OH from a CH_2Cl_2/MeOH/Et_2O mixed solvent at room temperature gave block-shaped crystals of **20**·$5.5CH_3OH$·$2H_2O$ which were suitable for X-ray crystallography.

Preparation of [Cu_2(μ-Gly-*n*-P)(XDK)(Mephen)$_2$] (Gly-*n*-P = glycerol *n*-phosphate, *n* = 2 (21), 3 (22)). A solution of Na_2[Gly-2-**P**] (17 mg, 0.051 mmol) in H_2O (3 mL)/CH_3OH (3 mL) was added to a solution of **6**·$1.5CH_2Cl_2$·CH_3OH (57 mg, 0.043 mmol) in methanol (8 mL). The reaction mixture was stirred overnight. The solvent was then removed to dryness, and the residue was extracted with CH_3OH (6 mL). The extract was passed through a glass filter, and Et_2O (1 mL) was slowly added to the extract. The solution was allowed to stand at 2 °C to produce pale blue crystals of [Cu_2(μ-Gly-2-**P**)(XDK)(Mephen)$_2$]·$2H_2O$ (**21**·$2H_2O$) (22 mg, 40%). Anal. Calcd for $C_{61}H_{69}O_{16}N_6Cu_2P$: C, 56.35; H, 5.35; N, 6.46. Found: C, 56.46; H, 5.28; N, 6.28. IR (KBr, cm^{-1}): 3398 (br), 1727 (s), 1684 (s), 1611 (s), 1360 (m), 1195 (m), 1086 (br), 725 (m). UV−vis (in CH_3OH): λ_{max} (ϵ) 716 nm (1.96×10^2 M^{-1} cm^{-1}). A similar procedure using Na_2[Gly-3-**P**] gave [Cu_2(μ-Gly-3-**P**)(XDK)(Mephen)$_2$]·$2H_2O$ (**22**·$2H_2O$) in a 29% yield. Anal. Calcd for $C_{61}H_{69}O_{16}N_6Cu_2P$: C, 56.35; H, 5.35; N, 6.46. Found: C, 56.37; H, 5.40; N, 6.32. IR (KBr, cm^{-1}): 3393 (br), 1728 (s), 1682 (s), 1611 (s), 1360 (m), 1194 (m), 1106 (br), 725 (m). UV−vis (in CH_3OH): λ_{max} (ϵ) 716 nm (1.95×10^2 M^{-1} cm^{-1}).

Preparation of [Cu_2(μ-Sugar-P)(XDK)(phen)$_2$] (Sugar-P = α-D-Glc-1-P (23a), D-Glc-6-P (24a), D-Man-6-P (25a), D-Fru-6-P (26a)) and [Cu_4(μ-D-Fru-1,6-P$_2$)(XDK)$_2$(phen)$_4$] (27a). A solution containing Na_2[α-D-Glc-1-**P**] (5.1 mg, 0.017 mmol) in a H_2O (1 mL)/CH_3OH (2 mL) mixed solvent was added to a solution of **4**·$2CH_2Cl_2$ (18 mg, 0.014 mmol) in methanol (10 mL). The reaction mixture was stirred for 12 h. The solvent was removed under reduced pressure to dryness, and the residue was extracted with CH_3OH (5 mL). The extract was passed through a glass filter, and Et_2O (0.5 mL) was added to the solution to yield pale blue microcrystals of [Cu_2(μ-α-D-Glc-1-**P**)(XDK)(phen)$_2$]·$12H_2O$ (**23a**·$12H_2O$; 9.9 mg, 46%). Anal. Calcd for $C_{62}H_{89}O_{29}N_6Cu_2P$: C, 48.34; H, 5.82; N, 5.46. Found: C, 48.54; H, 5.45; N, 5.56. IR (KBr, cm^{-1}): 3412 (s, br), 1727 (s), 1683 (s), 1614 (s), 1360 (m), 1196 (s, br), 724 (m). UV−vis (in CH_3OH): λ_{max} (ϵ) 732 nm (1.74×10^2 M^{-1} cm^{-1}). CD (in DMF): λ_{max} ($\Delta\epsilon$) 677 nm (2.34×10^{-1} M^{-1} cm^{-1}). Mass spectrum (ESI): *m*/*z* 1323.754 (MH^+, calcd 1323.281).

Pale blue microcrystals of [Cu_2(μ-D-Glc-6-**P**)(XDK)(phen)$_2$]·$7H_2O$ (**24a**·$7H_2O$), [Cu_2(μ-D-Man-6-**P**)(XDK)(phen)$_2$]·$10H_2O$ (**25a**·$10H_2O$), [Cu_2(μ-D-Fru-6-**P**)(XDK)(phen)$_2$]·$7H_2O$ (**26a**·$7H_2O$), and [Cu_4(μ-D-Fru-1,6-**P**$_2$)(XDK)$_2$(phen)$_4$]·$15H_2O$ (**27a**·$15H_2O$) were obtained using procedures simliar to those described above with Na_2[D-Glc-6-**P**], Na_2[D-Man-6-**P**], Na_2[D-Fru-6-**P**], and Na_n[D-Fru-1,6-**P**$_2$]. For **24a**·$7H_2O$, the yield was 26%. Anal. Calcd for $C_{62}H_{79}O_{24}N_6Cu_2P$: C, 51.34; H, 5.49; N, 5.79. Found: C, 50.93; H, 5.33; N, 5.58. IR (KBr, cm^{-1}): 3393 (s, br), 1728 (s), 1685 (s), 1613 (s), 1599 (s), 1359 (m), 1194 (m), 1106 (s, br), 723 (m). UV−vis (in CH_3OH): λ_{max} (ϵ) 739 nm (1.47×10^2 M^{-1} cm^{-1}). CD (in DMF): λ_{max} ($\Delta\epsilon$) 677 nm (4.42×10^{-1} M^{-1} cm^{-1}). Mass spectrum (ESI): *m*/*z* 1323.737 (MH^+, calcd 1323.281). For **25a**·$10H_2O$, the yield was 17%. Anal. Calcd for $C_{62}H_{85}O_{27}N_6Cu_2P$: C, 49.50; H, 5.69; N, 5.59. Found: C, 49.60; H, 5.33; N, 5.69. IR (KBr, cm^{-1}): 3404 (s, br), 1727 (s), 1683 (s), 1598 (s), 1360 (m), 1195 (m), 1091 (s, br), 724 (m). UV−vis (in CH_3OH): λ_{max} (ϵ) 731 nm (1.55×10^2 M^{-1} cm^{-1}). CD (in DMF): λ_{max} ($\Delta\epsilon$) 550 (-0.84×10^{-2}), 632 sh (9.15×10^{-2}), 719 nm (2.10×10^{-1} M^{-1} cm^{-1}). Mass spectrum (ESI): *m*/*z* 1323.276 (MH^+, calcd 1323.281). For **26a**·$7H_2O$, the yield was 36%. Anal. Calcd for $C_{62}H_{79}O_{24}N_6Cu_2P$: C,

Table 1. Crystallographic Data for Complexes **1a**, **1b**, **2a**, **3**, and **4**

	1a·2CH_3OH	**1b**·CH_3OH	**2a**·H_2O	**3**·4CH_2Cl_2	**4**·1.5CH_2Cl_2
formula	$C_{46}H_{79}N_7O_{14}Cu_2$	$C_{45}H_{75}N_6O_{10}ClCu_2$	$C_{42}H_{69}N_7O_{13}Cu_2$	$C_{56}H_{63}N_7O_{12}Cl_8Cu_2$	$C_{57.5}H_{58}N_7O_{12}Cl_3Cu_2$
fw	1081.26	1022.67	1007.14	1436.87	1272.58
cryst syst	monoclinic	orthorhombic	orthorhombic	triclinic	triclinic
space group	$P2_1/a$ (No. 14)	*Pbcn* (No. 60)	*Cmcm* (No. 63)	$P\bar{1}$ (No. 2)	$P\bar{1}$ (No. 2)
a (Å)	17.0927(5)	14.981(7)	15.063(7)	15.183(4)	14.203(1)
b (Å)	15.0100(5)	16.995(4)	16.132(7)	18.529(7)	18.0006(5)
c (Å)	20.8189(5)	20.765(6)	21.297(8)	11.838(4)	11.475(2)
α (deg)				101.53(3)	103.56(2)
β (deg)	93.2538(4)			103.25(3)	92.28(2)
γ (deg)				94.61(3)	80.32(2)
V (Å^3)	5332.7(3)	5287(2)	5175(3)	3148(2)	2811.5(5)
Z	4	4	4	2	2
T (°C)	−120	−118	−118	−119	−120
machine	AFC8R/Mercury	AFC7R	AFC7R	AFC7R	AFC8R/Mercury
μ(Mo Kα) (mm^{-1})	0.865	0.911	0.885	1.079	0.969
ρ_{calcd} (g cm^{-3})	1.347	1.285	1.293	1.516	1.503
2θ range (deg)	6−55	4−50	4−45	4−45	6−55
no. of unique data	9420 ($I > 2\sigma(I)$)	2595 ($I > 2\sigma(I)$)	1294 ($I > 2\sigma(I)$)	6554 ($I > 2\sigma(I)$)	8948 ($I > 2\sigma(I)$)
no. of params	668	332	195	767	749
R1[a]	0.051	0.078	0.059	0.049	0.066
wR2[b]	0.134	0.161	0.145	0.112	0.155

[a] $R1 = \sum||F_o| - |F_c||/\sum|F_o|$. [b] $wR2 = \{\sum[w(F_o^2 - F_c^2)^2/\sum[w(F_o^2)^2]\}^{1/2}$.

51.34; H, 5.49; N, 5.79. Found: C, 51.00; H, 5.12; N, 5.90. IR (KBr, cm^{-1}): 3393 (s, br), 1729 (s), 1685 (s), 1614 (s), 1359 (m), 1193 (m), 1105 (s, br), 723 (m). UV−vis (in CH_3OH): λ_{max} (ϵ) 727 nm (1.45×10^2 M^{-1} cm^{-1}). CD (in DMF): λ_{max} ($\Delta\epsilon$) 443 (8.57×10^{-2}), 655 (2.12×10^{-2}), 721 nm (1.88×10^{-2} M^{-1} cm^{-1}). Mass spectrum (ESI): *m*/*z* 1323.279 (MH$^+$, calcd 1323.281). For **27a**·15H_2O, yield 20%. Anal. Calcd for $C_{118}H_{148}O_{43}N_{12}Cu_4P_2$: C, 51.75; H, 5.45; N, 6.14. Found: C, 51.58; H, 5.34; N, 6.12. IR (KBr, cm^{-1}): 3384 (s, br), 1728 (s), 1683 (s), 1613 (s), 1359 (m), 1194 (m), 1105 (s, br), 724 (m). UV−vis (in CH_3OH): λ_{max} (ϵ) 720 nm (2.91×10^2 M^{-1} cm^{-1}). CD (in DMF): λ_{max} ($\Delta\epsilon$) 674 (-2.52×10^{-1}), 762 sh nm (-8.67×10^{-2} M^{-1}cm^{-1}).

Preparation of [Cu_2(*μ*-Sugar-P)(XDK)(Mephen)$_2$] (Sugar-P = α-D-Glc-1-P (23b), D-Glc-6-P (24b), D-Fru-6-P (26b)) and [Cu_4(*μ*-D-Fru-1,6-P_2)(XDK)$_2$(Mephen)$_4$] (27b). Following the procedure as described for **23a**, reactions of **6**·1.5CH_2Cl_2·CH_3OH with Na_2[α-D-Glc-1-**P**], Na_2[D-Glc-6-**P**], Na_2[D-Fru-6-**P**], and Na_n[D-Fru-1,6-$\mathbf{P}_2$] yielded pale blue microcrystals of [Cu_2(*μ*-α-D-Glc-1-**P**)(XDK)(Mephen)$_2$]·6H_2O (**23b**·6H_2O), [Cu_2(*μ*-D-Glc-6-**P**)(XDK)(Mephen)$_2$]·4CH_3OH·2H_2O (**24b**·4CH_3OH·2H_2O), [Cu_2(*μ*-D-Fru-6-**P**)(XDK)(Mephen)$_2$]·6H_2O (**26b**·6H_2O), and [Cu_4(*μ*-D-Fru-1,6-$\mathbf{P}_2$)(XDK)$_2$(Mephen)$_4$]·6CH_3OH·5H_2O (**27b**·6CH_3OH·5H_2O), respectively. For **23b**·6H_2O, the yield was 38%. Anal. Calcd for $C_{64}H_{81}O_{23}N_6Cu_2P$: C, 52.64; H, 5.59; N, 5.75. Found: C, 52.51; H, 5.58; N, 5.69. IR (KBr, cm^{-1}): 3426 (s, br), 1728 (w), 1683 (s), 1615 (s, br), 1361 (m), 1197 (m), 1091 (s, br), 727 (m). UV−vis (in CH_3OH): λ_{max} (ϵ) 722 nm (1.66×10^2 M^{-1} cm^{-1}). CD (in DMF): λ_{max} ($\Delta\epsilon$) 674 nm (1.33×10^{-1} M^{-1} cm^{-1}). Mass spectrum (ESI): *m*/*z* 1351.267 (MH$^+$, calcd 1351.312). For **24b**·4CH_3OH·2H_2O, the yield was 41%. Anal. Calcd for $C_{68}H_{89}O_{23}N_6Cu_2P$: C, 53.86; H, 5.92; N, 5.54. Found: C, 53.59; H, 6.15; N, 5.79. IR (KBr, cm^{-1}): 3411 (s, br), 1729 (w), 1684 (s), 1616 (s, br), 1360 (m), 1195 (m), 1090 (s, br), 800 (m). UV−vis (in CH_3OH): λ_{max} (ϵ) 720 nm (1.32×10^2 M^{-1} cm^{-1}). CD (in DMF): λ_{max} ($\Delta\epsilon$) 488 (-1.30×10^{-1}), 676 nm (2.62×10^{-1} M^{-1} cm^{-1}). Mass spectrum (ESI): *m*/*z* 1351.273 (MH$^+$, calcd 1351.312). For **26b**·6H_2O, the yield was 22%. Anal. Calcd for $C_{64}H_{81}O_{23}N_6Cu_2P$: C, 52.64; H, 5.59; N, 5.75. Found: C, 52.73; H, 5.61; N, 5.73. IR (KBr, cm^{-1}): 3413 (s, br), 1727 (w), 1685 (s), 1613 (s, br), 1360 (m), 1196 (m), 1087 (s, br), 725 (m). UV−vis (in CH_3OH): λ_{max} (ϵ) 717 nm (1.46×10^2 M^{-1} cm^{-1}). CD (in DMF): λ_{max} ($\Delta\epsilon$) 400 (1.21×10^{-2}), 573 (-1.46×10^{-2}), 657 sh (1.21×10^{-2}), 714 (2.48×10^{-2}), 768 sh nm (1.36×10^{-2} M^{-1} cm^{-1}). Mass spectrum (ESI): *m*/*z* 1351.271 (MH$^+$, calcd 1351.312). For **27b**·6CH_3OH·5H_2O, the yield was 20%. Anal. Calcd for $C_{128}H_{160}O_{39}N_{12}Cu_4P_2$: C, 54.77; H, 5.75; N, 5.99. Found: C, 54.49; H, 6.03; N, 6.19. IR (KBr, cm^{-1}): 3420 (s, br), 1730 (w), 1684 (s), 1615 (s, br), 1360 (m), 1194 (m), 1088 (s, br), 725 (m). UV−vis (in CH_3OH): λ_{max} (ϵ) 721 nm (2.51×10^2 M^{-1} cm^{-1}). CD (in DMF): λ_{max} ($\Delta\epsilon$) 434 sh (1.59×10^{-1}), 532 (-5.03×10^{-2}), 631 (-3.19×10^{-1}), 673 (-3.11×10^{-1}), 745 sh (-6.63×10^{-2}), 781 nm (1.04×10^{-1} M^{-1} cm^{-1}).

X-ray Crystallography. Crystals of **1a**·2CH_3OH, **1b**·CH_3OH, **2a**·H_2O, **3**·4CH_2Cl_2, **4**·1.5CH_2Cl_2, **5**·2CH_2Cl_2·CH_3OH·H_2O, **6**·CH_2Cl_2·2CH_3OH·0.5H_2O, **11**·2CH_3OH·2.5H_2O, **12**·2CH_2Cl_2·0.5CH_3OH·0.5H_2O, **13**·8CH_2Cl_2, **14**, **15**, **20**·5.5CH_3OH·2H_2O, and **27a**·8CH_3OH·11.75H_2O were mounted on top of glass fibers with Paraton N oil at low temperature. Crystal data and experimental conditions are summarized in Tables 1−3. Reflection data for **1b**, **2a**, **3**, **5**, **12**, and **15** were collected at −120 °C on a Rigaku AFC7R diffractometer equipped with graphite-monochromated Mo Kα (λ = 0.71069 Å) radiation. Three standard reflections were monitored every 150 reflections and showed no systematic decrease in intensity. Reflection data were corrected for Lorentz-polarization and absorption effects (ψ-scan method). Reflection data for **1a**, **4**, **6**, **11**, **13**, **14**, **20**, and **27a** were measured at −120 °C on a Rigaku AFC8R/Mercury CCD diffractometer equipped with graphite-monochromated Mo Kα radiation using a rotating-anode X-ray generator. A total of 1440 oscillation images, covering the whole sphere of $2\theta < 52°$, were collected with exposure rates of 120 (**6**, **13**) and 240 (**11**) s/deg by the ω-scan method ($-70 < \omega < 110°$) with a $\Delta\omega$ of 0.25°. For **1a**, **4**, **14**, **20**, and **27a**, a total of 2160 oscillation images, covering the whole sphere of $2\theta < 55°$, were collected with exposure rates of 120−128 s/deg by the ω-scan method ($-62 < \omega < 118°$) with a $\Delta\omega$ of 0.25°. The crystal-to-detector (70 × 70 mm) distance was set to 60 mm. The data were processed using Crystal Clear 1.3.5 (Rigaku/MSC)[17] and corrected for Lorentz-polarization and absorption effects.

(17) *Crystal Clear*, version 1.3.5; Rigaku and Molecular Structure Corp.: The Woodlands, TX, 2003.

Table 2. Crystallographic Data for Complexes **5**, **6**, **11**, and **12**

	5·$2CH_2Cl_2$·CH_3OH·H_2O	**6**·CH_2Cl_2·$2CH_3OH$·$0.5H_2O$	**11**·$2CH_3OH$·$2.5H_2O$	**12**·$2CH_2Cl_2$·$0.5CH_3OH$·$0.5H_2O$
formula	$C_{59}H_{73}N_7O_{14}Cu_2Cl_4$	$C_{61}H_{70}N_7O_{14.5}Cl_2Cu_2$	$C_{66}H_{77}N_7O_{19.5}Cu_2P$	$C_{70.5}H_{71}N_7O_{16}Cl_4Cu_2P$
fw	1373.17	1331.26	1438.44	1572.25
cryst syst	triclinic	monoclinic	monoclinic	triclinic
space group	$P\bar{1}$ (No. 2)	$P2_1/c$ (No. 14)	$C2/c$ (No. 15)	$P\bar{1}$ (No. 2)
a (Å)	13.128(3)	12.972(1)	31.485(5)	16.564(7)
b (Å)	19.642(3)	19.444(2)	27.913(3)	18.324(5)
c (Å)	12.872(2)	26.732(3)	20.226(3)	13.000(4)
α (deg)	95.58(1)			98.28(2)
β (deg)	95.72(2)	95.026(6)	120.970(4)	102.98(3)
γ (deg)	101.43(1)			98.08(3)
V (Å^3)	3213(1)	6716(1)	15240(4)	3743(2)
Z	2	4	8	2
T (°C)	−116	−120	−120	−118
machine	AFC7R	AFC8R/Mercury	AFC8R/Mercury	AFC7R
μ(Mo Kα) (mm^{-1})	0.895	0.778	0.648	0.801
ρ_{calcd} (g cm^{-3})	1.419	1.316	1.254	1.395
2θ range (deg)	4−45	6−52	6−52	4−50
no. of unique data	6173 ($I > 2\sigma(I)$)	7350 ($I > 2\sigma(I)$)	4732 ($I > 2\sigma(I)$)	9512 ($I > 2\sigma(I)$)
no. of params	761	815	503	965
R1[a]	0.077	0.080	0.103	0.069
wR2[b]	0.172	0.165	0.215	0.153

[a] $R1 = \sum||F_o| - |F_c||/\sum|F_o|$. [b] $wR2 = \{\sum[w(F_o^2 - F_c^2)^2/\sum[w(F_o^2)^2]\}^{1/2}$.

Table 3. Crystallographic Data for Complexes **13**−**15**, **20**, and **27a**

	13·$8CH_2Cl_2$	**14**	**15**	**20**·$5.5CH_3OH$·$2H_2O$	**27a**·$8CH_3OH$·$11.75H_2O$
formula	$C_{76}H_{78}N_9O_{19}Cu_2PCl_{16}$	$C_{48}H_{44}N_6O_{14}Cu_2P_2$	$C_{36}H_{48}N_{10}O_{22}Cu_2P_2$	$C_{68.5}H_{88}N_7O_{22.5}Cu_2P$	$C_{125.5}H_{173.5}N_{12}O_{47.75}Cu_4P_2$
fw	2146.81	1117.95	1161.87	1527.55	2930.43
cryst syst	monoclinic	monoclinic	triclinic	triclinic	monoclinic
space group	$P2_1/n$ (No. 14)	$P2_1/c$ (No. 14)	$P\bar{1}$ (No. 2)	$P\bar{1}$ (No. 2)	$C2$ (No. 5)
a (Å)	14.401(1)	11.384(2)	9.849(2)	12.521(3)	30.928(1)
b (Å)	23.416(2)	19.612(2)	14.252(3)	16.704(4)	32.894(1)
c (Å)	27.261(3)	11.210(1)	8.944(2)	18.427(5)	37.034(2)
α (deg)			106.94(2)	91.105(2)	
β (deg)	98.033(5)	105.062(4)	100.49(1)	106.131(3)	105.942(2)
γ (deg)			89.71(2)	94.116(4)	
V (Å^3)	9102(1)	2416.6(5)	1179.3(4)	3689(1)	36227(3)
Z	4	2	1	2	8
T (°C)	−120	−120	−118	−120	−120
machine	AFC8R/Mercury	AFC8R/Mercury	AFC7R	AFC8R/Mercury	AFC8R/Mercury
μ(Mo Kα) (mm^{-1})	1.025	1.021	1.063	0.676	0.549
ρ_{calcd} (g cm^{-3})	1.566	1.536	1.636	1.375	1.074
2θ range (deg)	6−52	6−55	4−50	6−55	6−52
no. of unique data	9472 ($I > 2\sigma(I)$)	3546 ($I > 2\sigma(I)$)	3691 ($I > 2\sigma(I)$)	11278($I > 2\sigma(I)$)	46995 ($I > 2\sigma(I)$)
no. of params	1109	326	326	929	2019
R1[a]	0.091	0.052	0.024	0.067	0.093
wR2[b]	0.194	0.117	0.065	0.153	0.213

[a] $R1 = \sum||F_o| - |F_c||/\sum|F_o|$. [b] $wR2 = \{\sum[w(F_o^2 - F_c^2)^2/\sum[w(F_o^2)^2]\}^{1/2}$.

The structures of **1a**, **1b**, **2a**, **3**-**6**, **12**−**15**, and **20** were solved by direct methods with SIR92[18] and were refined with full-matrix least-squares techniques on F^2 using teXsan.[19] In the structures of **1a**, **3**, **5**, and **6**, all non-hydrogen atoms, except those of the nitrate anion and solvated methanol (**1a**) and of solvated methanol and water (**5**, **6**), were refined with anisotropic thermal parameters. The positions of the C−H hydrogen atoms were calculated, and those of the hydroxo H atom were determined by difference Fourier syntheses. In the structures of **1b** and **2a**, the tetmen and tmen ligands were disordered with respect to the Cu_2O plane and were refined by using a two-site model with 0.5 occupancy. All non-hydrogen atoms, except those of nitrate anion and the solvent water molecule (**2a**), were refined with anisotropic thermal parameters. The positions of the C−H hydrogen atoms were calculated and the hydroxo H atoms were not found from difference Fourier maps. In the structure of **4**, the Cu, O, and N atoms included in the complex cations were refined anisotropically and other non-hydrogen atoms were refined with isotropic temperature factors. The position of the hydroxo H atom in **4** was determined from difference Fourier maps. In the structure of **11**, the Cu, P, O, and N atoms involved in the complex cation were refined anisotropically, and other non-hydrogen atoms were refined with isotropic thermal factors. In the structures of **12**−**15** and **20**, all non-hydrogen atoms were refined with anisotropic thermal parameters and the positions of C−H hydrogen atoms were calculated and fixed in the refinement. The structure of **27a** was solved by the Patterson

(18) Burla, M. C.; Camalli, M.; Cascarano, G.; Giacovazzo, C.; Polidori, G.; Spagna, R.; Viterbo, D. *J. Appl. Crystallogr.* **1989**, *22*, 389.
(19) *TEXSAN: Crystal Structure Analysis Package*; Molecular Structure Corp.: The Woodlands, TX, 1999.

Scheme 1

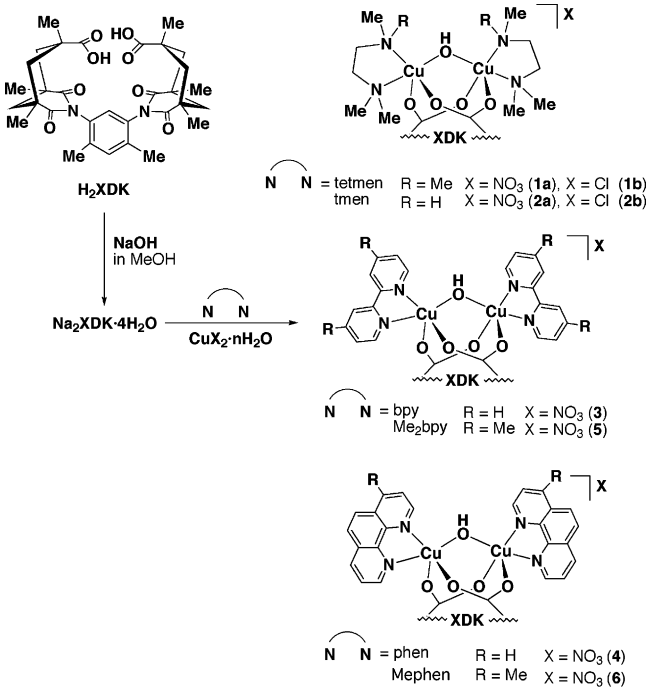

method with DIRDIF94 PATTY[20] and was refined with full-matrix least-squares techniques on F^2 with SHELXL-97.[21] The Cu and P atoms were refined anisotropically, and the other non-hydrogen atoms were refined with isotropic temperature factors. The C−H hydrogen atoms were calculated, and the H atoms for hydroxyl groups of the sugar moieties were not determined. The inherent weak reflection data in the high-angle region and the existence of two independent, large, complex molecules in the asymmetric unit may result in the low quality of the present structure determination. The relatively low calculated density indicated that a number of solvent molecules were still not determined.

All calculations were carried out on Silicon Graphics Indigo and O2 Stations with the teXsan program system and on a Pentium PC with the Crystal Structure package.[22]

Results and Discussion

Hydroxo-Bridged Dinuclear Copper(II) Complexes with Biscarboxylate Ligand XDK, [Cu$_2$(μ-OH)(XDK)(L)$_2$]X. (i) Syntheses. Reactions of $Na_2XDK{\cdot}4H_2O$ with $CuX_2{\cdot}nH_2O$ (X = NO_3, Cl) in the presence of diamine (tetmen, tmen) and diimine (bpy, phen, Me_2bpy, Mephen) auxiliary ligands yielded a series of discrete (μ-hydroxo)bis(μ-carboxylato)dicopper(II) complexes, [Cu$_2$(μ-OH)(XDK)(L)$_2$]X (L = tetmen, X = NO_3 (**1a**), Cl (**1b**); L = tmen, X = NO_3 (**2a**), Cl (**2b**); X = NO_3, L = bpy (**3**), phen (**4**), Me_2bpy (**5**), Mephen (**6**)) (Scheme 1). All the complexes were isolated as pure crystalline forms in good yields (37−93%). Since deoxy hemerythrin has been shown to contain a (μ-hydroxo)bis(μ-carboxylato)diiron(II) active site, a number of model complexes with redox-active dinuclear Fe and Mn ions have been synthesized;[1] however, analogous dinuclear copper(II) complexes consisting of the (μ-hydroxo)bis(μ-carboxylato)dimetal framework are extremely rare, presumably because of the formation of polymeric compounds with versatile bridging systems of carboxylate ligands. The only available examples are [Cu$_2$(μ-OH)(μ-PhCOO)$_2$(tetmen)$_2$](PF_6) (**8a**)[23] and [Cu$_2$(μ-OH)(μ-HCOO)$_2$(bpy)$_2$](BF_4) (**8b**),[24] on the basis of Cambridge Crystal Structure Database. The present results demonstrated that the dinucleating biscarboxylate ligand XDK is remarkably effective for constructing the deoxy hemerythrin-type dicopper(II) platform. The ESI mass spectra of **1**−**6** in CH_3OH or CH_2Cl_2 exhibited the parent monocationic peaks assignable to [Cu$_2$(μ-OH)(XDK)(L)$_2$]$^+$ (m/z = 953.45 (**1a**), 925.43 (**2a**), 1033.24 (**3**), 1081.25 (**4**), 1089.31 (**5**), 1109.31 (**6**)), indicating that the dinuclear structures are retained in the solutions. The detailed structures of **1a**, **b**, **2a**, and **3**−**6** were determined by X-ray crystallography.

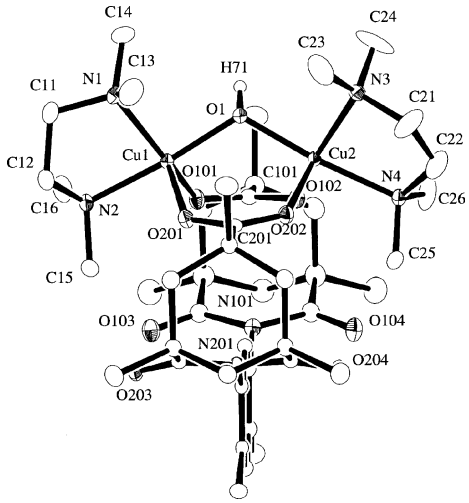

Figure 1. ORTEP drawing for the complex cation of **1a**.

(ii) Structures. ORTEP plot for the complex cation of **1a** is illustrated in Figure 1 (ORTEP diagrams for the complex cations of **1b**, **2a**, and **3**−**6** are shown in Figures S2−S7 in the Supporting Information), and the structural parameters for **1a**, **b**, **2a**, and **3**−**6** are summarized in Table 4. All the complexes are composed of dinuclear Cu(II) centers that are bridged by a hydroxo group and two carboxylates of XDK ligand. The terminal sites of each Cu(II) ion are capped with a chelating N-donor ligand to result in a [CuO_3N_2] five-coordinate environment. The structure of complex **1a** possesses a pseudo-C_s symmetry with the mirror plane vertical to the Cu_2O triangle, and both the N atoms (N_c) occupying cis positions to the hydroxo oxygen atom (O_b) are tilted in the same side with respect to the Cu_2O plane (Figures 1 and 2a). The Cu···Cu interatomic distance is 3.2910(4) Å, which is longer by 0.062 Å than that in [Cu$_2$(μ-OH)(PhCOO)$_2$(tetmen)$_2$]PF_6 (**8a**) (3.229(1) Å),[23] mainly because of the slightly larger Cu−O_b−Cu angle (117.63(9)°) compared to

(20) Beurskens, P. T.; Admiraal, G.; Beurskens, G.; Bosman, W. P.; de Gelder, R.; Israel, R.; Smits, J. M. M. *DIRDIFF-94 Program System*; Technical Report of the Crystallography Laboratory; University of Nijmegen: Nijmegen, The Netherlands, 1994.
(21) Sheldrick, G. M. *SHELXL-97: Program for the Refinement of Crystal Structures*; University of Göttingen: Göttingen, Germany, 1996.
(22) *Crystal Structure 3.6: Crystal Structure Analysis Package*; Rigaku and Molecular Structure Corp.: The Woodlands, TX, 2003.
(23) Geetha, K.; Nethaji, M.; Chakravarty, A. R.; Vasanthacharya, N. Y. *Inorg. Chem.* **1996**, *35*, 7666.
(24) Tokii, T.; Nagamatsu, M.; Hamada, H.; Nakashima, M. *Chem. Lett.* **1992**, 1091.

Table 4. Structural Parameters of the Dicopper(II) Complexes with $\{(\mu\text{-Hydroxo})\text{bis}(\mu\text{-carboxylato})Cu_2\}^{+}$ Core[a]

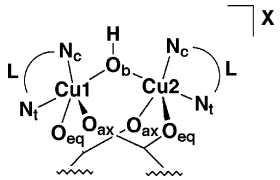

	1a	1b	2a	3	4	5	6	8a[b]	8b[c]
L	tetmen	tetmen	tmen	bpy	phen	Me_2bpy	Mephen	tetmen	bpy
X	NO_3	Cl	NO_3	NO_3	NO_3	NO_3	NO_3	PF_6	BF_4
				bond lengths (Å)					
Cu1···Cu2	3.2910(4)	3.264(2)	3.274(2)	3.2100(8)	3.1624(6)	3.205(1)	3.2034(9)	3.229(1)	3.171(1)
av Cu−O_b	1.924	1.925(3)	1.913(3)	1.909	1.899	1.906	1.915	1.930	1.928
Cu1−O_b	1.921(2)			1.911(3)	1.903(2)	1.907(4)	1.907(3)	1.925(6)	1.927(4)
Cu2−O_b	1.926(2)			1.907(3)	1.895(3)	1.905(4)	1.923(3)	1.934(5)	1.928(4)
av Cu−N_t	2.058	2.016(6)	2.037(7)	1.989	2.012	1.976	1.989	2.051	2.008
Cu1−N_t	2.038(2)			1.994(4)	2.013(3)	1.965(5)	1.990(4)	2.050(6)	2.004(5)
Cu2−N_t	2.077(2)			1.983(4)	2.011(3)	1.987(5)	1.988(4)	2.051(8)	2.012(5)
av Cu−N_c	2.096	2.11[f]	2.04(1)[f]	2.049	2.071	2.028	2.045	2.107	2.020
Cu1−N_c	2.112(2)			2.034(4)	2.078(3)	2.042(6)	2.058(4)	2.106(7)	2.027(5)
Cu2−N_c	2.079(2)			2.064(4)	2.064(3)	2.014(6)	2.032(5)	2.107(7)	2.012(5)
av Cu−O_{eq}	2.017			2.024	2.036	2.020	1.981	1.990	1.999
Cu1−O_{eq}	2.029(2)	2.068(5)	2.086(4)[g]	2.012(3)	2.054(2)	2.059(5)	1.984(3)	1.991(6)	2.029(5)
Cu2−O_{eq}	2.005(2)			2.035(3)	2.017(2)	1.981(4)	1.977(4)	1.988(6)	1.968(5)
av Cu−O_{ax}	2.198			2.118	2.082	2.130	2.181	2.131	2.165
Cu1−O_{ax}	2.192(2)	2.136(4)	2.086(4)[g]	2.144(3)	2.063(2)	2.087(4)	2.193(4)	2.128(6)	2.140(5)
Cu2−O_{ax}	2.204(2)			2.091(4)	2.101(2)	2.173(4)	2.168(4)	2.134(6)	2.190(5)
				bond angles (deg)					
Cu1−O_b−Cu2	117.63(9)	116.0(3)	117.7(3)	114.5(2)	112.7(1)	114.4(2)	113.5(2)	113.6(3)	110.7(2)
av O_b−Cu−N_t	174.04	175.4(2)	176.1(3)	174.2	173.7	174.9	175.1	167.4	167.8
O_b−Cu1−N_t	174.18(8)			173.4(2)	174.1(1)	176.0(2)	178.8(2)	169.5(3)	172.8(2)
O_b−Cu2−N_t	173.89(8)			175.0(2)	173.3(1)	173.8(2)	171.3(2)	165.3(3)	162.8(2)
av O_b−Cu−N_c	93.01	91.0[f]	91.6(3)[f]	95.1	93.6	96.0	95.4	91.7	
O_b−Cu1−N_c	93.02(8)			94.3(2)	93.4(1)	97.7(2)	97.8(1)	91.6(2)	
O_b−Cu2−N_c	93.00(8)			95.9(1)	93.7(1)	94.3(2)	92.9(2)	91.7(3)	
av N_t−Cu−N_c	84.59	85.0[f]	84.7(3)[f]	80.0	80.6	80.3	80.9	84.4	
N_t−Cu1−N_c	84.64(9)			80.1(2)	80.7(1)	79.6(2)	81.1(2)	84.5(3)	
N_t−Cu2−N_c	84.54(8)			79.8(2)	80.5(1)	80.9(2)	80.6(2)	84.2(3)	
av N_c−Cu−O_{eq}	149.97	146.3 [f]	143.4(4) [f]	134.3	132.3	135.8	151.3	161.1	157.7
N_c−Cu1−O_{eq}	148.80(9)			140.4(2)	131.2(1)	119.5(2)	154.6(2)	160.1(3)	147.2(2)
N_c−Cu2−O_{eq}	151.14(8)			128.1(2)	133.4(1)	152.0(2)	148.0(2)	162.0(3)	168.2(2)
av N_c−Cu−O_{ax}	98.44	100.2 [f]	104.4(4) [f]	112.0	110.0	111.2	92.9	97.5	
N_c−Cu1−O_{ax}	99.90(9)			109.3(1)	111.4(1)	123.0(2)	87.0(1)	98.7(3)	
N_c−Cu2−O_{ax}	96.98(8)			114.7(2)	108.6(1)	99.3(2)	98.8(2)	96.3(3)	
av O_{eq}−Cu−O_{ax}	110.78	112.4(2)	111.7(2)	112.0	116.3	110.5	113.8	99.5	
O_{eq}−Cu1−O_{ax}	110.48(7)			108.4(1)	116.1(1)	115.1(2)	116.2(1)	99.3(2)	
O_{eq}−Cu2−O_{ax}	111.08(7)			115.6(1)	116.5(1)	105.9(2)	111.3(1)	99.7(2)	
τ (Cu1)[d]	0.42	0.48/0.50[f]	0.55	0.55	0.72	0.88	0.40	0.16	0.43
τ (Cu2)[d]	0.38			0.78	0.67	0.36	0.39	0.06	0.09
$\sum$ Cu−O_b−Z (deg)[e]	344.73	327.7	g	336.6	314.9	341.8	349.2	332.6	g

[a] The atom labeling is shown in the chart. O_{ax} and O_{eq} are the carboxylate oxygen atoms at the apical and basal positions of the pseudo-square pyramidal structure around the Cu atoms. [b] Ref 23 for $[Cu_2(\mu\text{-OH})(\mu\text{-PhCOO})_2(\text{tetmen})_2](PF_6)$ (**8a**). [c] Ref 24 for $[Cu_2(\mu\text{-OH})(\mu\text{-HCOO})_2(\text{bpy})_2](BF_4)$ (**8b**). [d] $\tau = (\beta - \alpha)/60$, where α is the second largest basal angle and β is the largest basal angle (ref 25). [e] $\sum$ Cu−O_b−Z is the summation of three Cu−O_b−Z angles (Z = Cu, H). [f] The N_c atom is disordered, and the O_{eq} and O_{ax}atoms are crystallographically identical. [g] Not determined.

that of **8a** (113.6(3)°). The sum of the three bond angles around the O_b atom is 344.73°, suggesting that the sp^3 character of the bridging O atom appreciably decreases in **1a** compared to **8a** (332.6°). The N_2O_3 arrangement around the copper centers is essentially recognized as square-pyramidal geometry with the O201 and O202 atoms occupying the respective apical positions, but the structures are considerably distorted toward trigonal-bipyramidal geometry as indicated by τ values[25] of 0.42 (Cu1) and 0.38 (Cu2). Although the severely disordered structures of the tetmen and tmen ligands prevent detailed discussion, the $\{Cu_2(\mu\text{-OH})(\mu\text{-RCO}_2)_2\}^{+}$ core structures of **1b** and **2a** are similar to that of **1a** (Table 4 and Figures S2 and S3).

In complexes **3**−**6** with diimine ligands, the Cu···Cu separation is noticeably reduced to 3.1624(6)−3.2100(8) Å, which is in accord with the shorter average Cu−O_b distances (1.899−1.915 Å) and the smaller Cu−O_b−Cu angles (112.7(1)−114.5(2)°) compared with those of the diamine complexes. Among them, complex **4** with phen exhibits the shortest Cu···Cu distance of 3.1624(6) Å which is slightly shorter than that of **8b** (3.171(1) Å).[24] The Cu−O_b−Cu angle

(25) Addison, A. W.; Rao, T. N. *J. Chem. Soc., Dalton Trans*. **1984**, 1349.

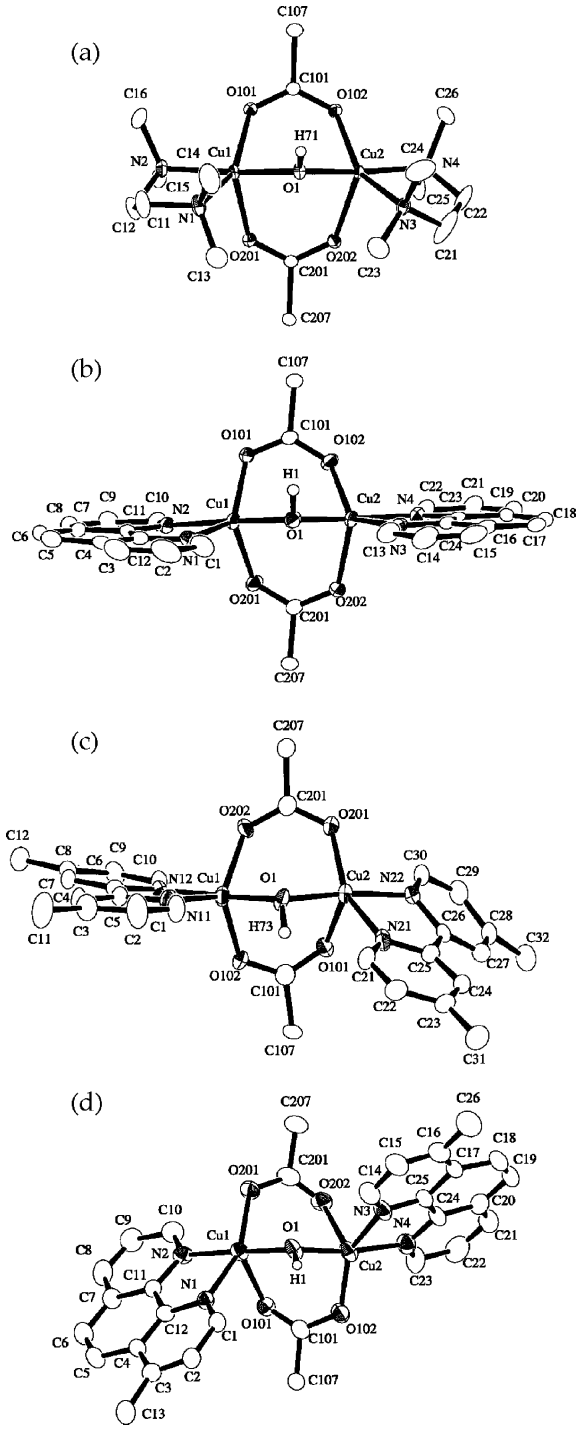

Figure 2. The dicopper(II) structures of (a) **1a**, (b) **4**, (c) **5**, and (d) **6** viewed along the Cu_2O plane. XDK, except for the carboxylate groups, is omitted for clarity.

of **4** is small (112.7(1)°), and the sum of the three bond angles around the O_b atom (314.9°) is also small in comparison with the corresponding values of other diimine complexes (336.6° (**3**), 341.8° (**5**), 349.2° (**6**)), indicating the sp^3 character of the bridging oxygen in **4**. The geometry of the five-coordinate copper(II) atoms delicately varied depending on the diimine ligands (Figure 2). In complexes **3** and **4**, both the Cu(II) centers essentially adopt the trigonal-bipyramidal geometry with the O_b and N_t atoms occupying the apical sites (τ = 0.55−0.78) (Figure 2b). In complex **5** with Me_2bpy, the Cu1 atom takes a trigonal-bipyramidal geometry ($\tau = 0.88$), and the Cu2 sits in a square-pyramidal environment ($\tau = 0.36$), resulting in an asymmetric dinuclear structure (Figure 2c). In complex **6** with Mephen, both Cu atoms have distorted square-pyramidal structures (τ = 0.39−0.40) with the apical O101 and O202 atoms, resulting in a pseudo-C_2 symmetrical structure (Figure 2d).

Table 5. Electrochemical Data for Complexes **1**−**6**[a]

complex	E_{pc} (V)[b]
1a	−1.24
1b	−1.27
2a	−1.34
2b	−1.29
3	−1.07
4	−1.11
5	−1.09
6	−1.09

[a] Measured in acetonitrile containing 0.1 M [nBu$_4$N][PF$_6$] at a scan rate of 100 mV/s. [b] Referenced to the redox potentioal of Ag/AgPF$_6$ in acetonitrile.

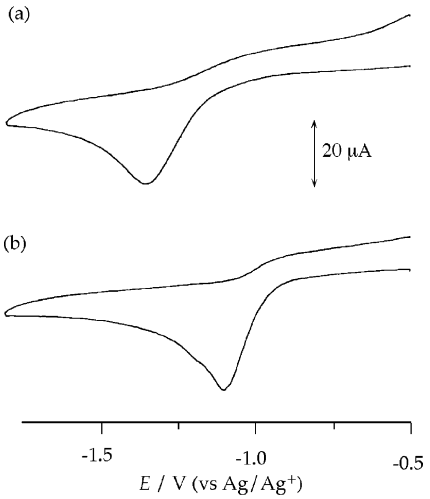

Figure 3. Cyclic voltammograms obtained for (a) **1a** and (b) **5** in CH_3CN (0.1 M [nBu$_4$N][PF$_6$]) at a scan rate of 100 mV s^{-1}.

(iii) Electrochemical and Magnetic Properties. The electrochemical properties of complexes **1**−**6** were analyzed by cyclic voltammetry (Table 5 and Figure 3). The cyclic voltammograms (CV) of **1a**, **b**, **2a**, and **b** in acetonitrile solution showed an irreversible reduction wave around E_{pc} = −1.24 to −1.34 V, assignable to a two-electron reduction process, [Cu^{II}_2] → [Cu^{I}_2], on the basis of coulometric analysis. For complexes **3**−**6**, the similar irreversible reduction occurred at more positive potentials, around E_{pc} = −1.07 to −1.11 V, which is consistent with the lesser electron-donating ability of the diimine ligands compared with diamines. The reduction peak potentials of **3**−**6** were not sensitive to the diimine ligands, as well as the copper(II) coordination geometry. Some attemps to isolate dicopper(I) complexes by chemical and electrochemical reduction of **1a** and **3** were not successful, whereas a series of dinuclear copper(I) ions have been stabilized by the biscarboxylate ligand XDK.[12i]

The temperature-dependent magnetic susceptibility data were analyzed by least-squares fitting procedures using the Bleany−Bowers equation based on the Hamiltonian H =

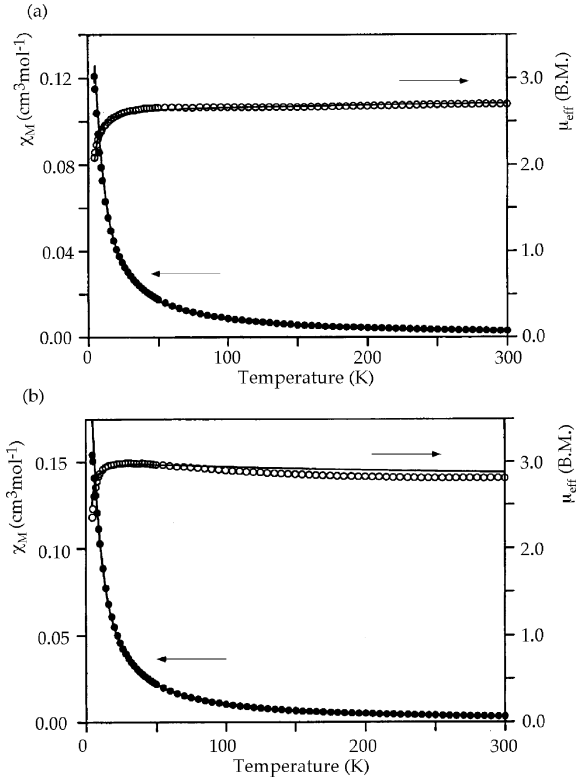

Figure 4. Plots of molar susceptibility, χ_M (●), and effective magnetic moment, μ_{eff} (○), vs T for (a) **3** and (b) **4** with the fitted data (—).

$-2JS_1S_2$ (Figure 4).[16] The best-fitted parameters are obtained as follows: $2J = -49.2$ cm^{-1}, $g = 2.07$ for **1a**, $2J = -4.2$ cm^{-1}, $g = 2.17$ for **3**, $2J = 52.0$ cm^{-1}, $g = 2.21$ for **4**, and $2J = -5.4$ cm^{-1}, $g = 2.09$ for **5**. For all complexes, except **4**, the negative values of $2J$ are indicative of intramolecular antiferromagnetic exchange interactions. While no definite magnetostructural correlation has been established because of the paucity of characterized examples with (μ-hydroxo)bis(μ-carboxylato)dicopper(II) complexes, it has been observed that the geometry at the endogeneous bridging oxygen atom could be an important indicator in predicting the major pathway for the spin−spin coupling; the sp^2 character of the bridging oxygen enhances antiferromagnetic interaction, and sp^3 character may reduce it.[23,26] The values for the sum of angles at the monatomic bridging oxygen (Table 4) might indicate such a tendency with the observed J values; however, this interpretation potentially involves large errors accompanied by the position of the X-ray determined hydrogen atom. In general, for bis(μ-hydroxo)dicopper(II) complexes, the well-known empirical magnetostructural correlation has been developed as follows: the Cu−OH−Cu pathway with a Cu−O−Cu angle larger than 97.5° mostly transfers antiferromagnetic interactions, and the pathway with a Cu−O−Cu angle less than 97.5° transfers ferromagnetic interactions.[27] While the observed J values are composed of ferromagnetic and antiferromagnetic interactions, both of which are influenced by a variety of structural and electronic factors, magnetic interactions between the two copper ions

Chart 1

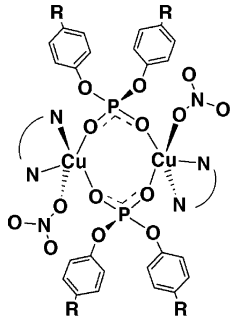

are assumed to be effective through the Cu−O−Cu pathway in complexes **1a**, **3**, **4**, and **5**, considering that the magnetic orbitals are $d_{x^2-y^2}$ and d_{z^2}, respectively, for square pyramidal and trigonal bipyramidal Cu(II) ions.[27b,c] In fact, although the values are larger than 100°, the Cu−O−Cu angles were revealed to have a delicate correlation with the J values in the present case. The entirely different magnetic interactions observed with the same N-donor ligand (tetmen) in **1a** ($2J = -49.2$ cm^{-1}) and **8a** ($2J = 45.1$ cm^{-1}) are rationalized with the values for the Cu−O−Cu angles of 117.63(9)° (**1a**) and 113.6(3)° (**8a**). For complex **4** (Cu−O−Cu = 112.7(1)°), the positive $2J$ value (52.0 cm^{-1}) indicated a moderate ferromagnetic interaction between the two copper(II) ions, which is, interestingly, in contrast with the small antiferromagnetic interactions, $2J = -4.2$ and -5.4 cm^{-1}, for **3** (Cu−O−Cu = 114.5(2)°) and **5** (Cu−O−Cu = 114.4(2)°), respectively. These results demonstrated that the spin−spin coupling interaction is remarkably sensitive to the Cu−OH−Cu angle in the (μ-hydroxo)bis(μ-carboxylato)dicopper(II) complexes.

Reactions of Hydroxo-Bridged Dicopper Complexes with Organic Phosphate Diesters. Complex **4** readily reacted with diphenyl phosphoric acid (HDPP) or bis(4-nitrophenyl) phosphoric acid (HBNPP) in dichloromethane to produce [Cu$_2$(μ-η^1,η^1-(RO)$_2$PO$_2$)(XDK)(phen)$_2$]NO$_3$ (R = Ph (**12**), 4-NO$_2$Ph (**13**)) in good yields. During the reaction, the phosphate diesters were not hydrolyzed and simply introduced onto the dinuclear core as bridging ligands. The reaction of **3** with HDPP also gave the similar complex, [Cu$_2$(μ-η^1,η^1-(PhO)$_2$PO$_2$)(XDK)(bpy)$_2$] NO$_3$ (**11**); however, that with HBNPP under the same conditions resulted in the dissociation of XDK from the dinuclear core. When complex **5** was treated with HDPP, the XDK dissociated dicopper(II) complex, [Cu$_2$(μ-η^1,η^1-(PhO)$_2$PO$_2$)(NO$_3$)$_2$(Me$_2$bpy)$_2$] (**14**), was isolated. A similar complex, [Cu$_2$(μ-η^1,η^1-(4-NO$_2$-PhO)$_2$PO$_2$)(NO$_3$)$_2$(tetmen)$_2$] (**15**), was also isolated from the reaction of **1a** with HBNPP (Chart 1). These results suggested that the XDK-bridged dicopper centers with phen terminal ligands could be suitable for fixing the phosphate

(26) Mazurek, W.; Kennedy, B. J.; Murray, K. S.; O'Connor, M. J.; Rodgers, J. R.; Snow, M. R.; Wedd, A. G.; Zwack, P. R. *Inorg. Chem.* **1985**, *24*, 3258.

(27) (a) Crawford, V. H.; Richardson, H. W.; Wasson, J. R.; Hodgson, D. J.; Hatfield, W. E. *Inorg. Chem.* **1976**, *15*, 2107. (b) Christou, G.; Perlepes, S. P.; Libby, E.; Folting, K.; Huffman, J. C.; Webb, R. J.; Hendrickson, D. N. *Inorg. Chem.* **1990**, *29*, 3657. (c) Youngme, S.; Chailuecha, C.; van Albada, G. A.; Pakawatchai, C.; Chaichit, N.; Reedjik, J. *Inorg. Chim. Acta* **2005**, *358*, 1068.

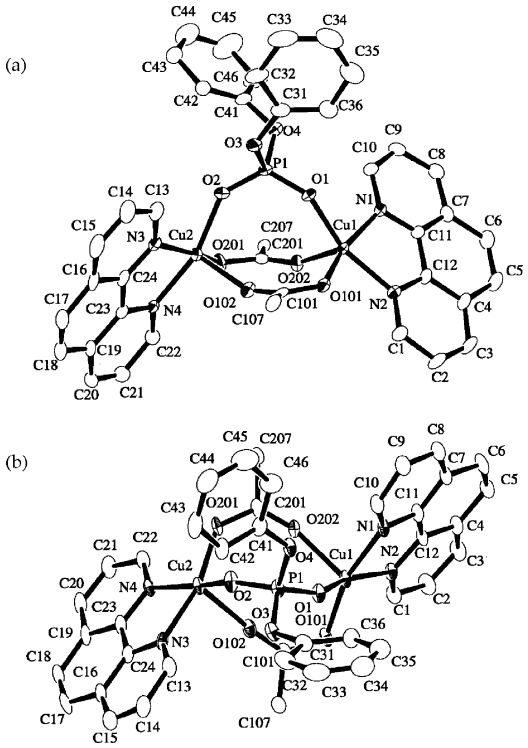

Figure 5. ORTEP plots for the complex cation of **12** viewed (a) vertical to and (b) along the PO_2 plane. XDK, except for the carboxylate groups, is omitted for clarity.

diesters as a bridging unit, and in addition, the XDK-bridged dicopper(II) complexes with the stronger N-donors, tetmen and Me_2bpy, are likely to be decomposed by dissociation of the XDK ligand in the treatment with organic phosphoric acids.

The detailed structures of **11**−**13** were determined by X-ray crystallography. ORTEP plots for the core structure of complex **12** are illustrated in Figure 5, and selected bond distances and angles of complexes **11**−**13** are listed in Table 6 (ORTEP plots for the complex cations of **11**−**13** are supplied as Supporting Information Figures S8−S10). The structure of **12** possesses a pseudo-C_2 symmetry (Figure 5b) and is composed of two copper atoms triply bridged by two carboxylate groups of XDK and a phosphate unit of the DPP ligand. The terminal sites of each copper ion are occupied by the N atoms of phen to result in N_2O_3 five-coordinated square-pyramidal environments ($\tau = 0.04$ for Cu1 and 0.03 for Cu2). While several discrete dicopper structures involving bridging phosphate esters and their related compounds have been synthesized by utilizing alkoxo-, phenoxo-, diimine-, and polyamine-based dinucleating ligands,[28−32] the present

Table 6. Selected Bond Distances and Angles for **11**, **12**, and **13**[a]

	11	**12**	**13**
	bond distances (Å)		
Cu1···Cu2	4.268(3)	4.2685(8)	4.315(1)
Cu1−O1	1.980(7)	1.966(3)	1.964(5)
Cu2−O2	1.999(8)	1.954(3)	1.989(5)
Cu1−O101	1.954(7)	1.942(3)	1.940(5)
Cu1−O202	2.177(10)	2.164(3)	2.181(5)
Cu2−O102	2.211(9)	2.182(3)	2.143(5)
Cu2−O201	1.944(7)	1.921(3)	1.933(5)
Cu1−N1	2.045(9)	2.029(4)	2.034(6)
Cu1−N2	2.02(1)	1.997(3)	1.981(6)
Cu2−N3	2.044(10)	2.037(3)	2.033(6)
Cu2−N4	2.00(1)	1.998(3)	2.005(6)
	bond angles (deg)		
O1−Cu1−O101	92.9(3)	92.7(1)	93.1(2)
O1−Cu1−O202	96.8(3)	94.9(1)	90.7(2)
O1−Cu1−N1	90.8(3)	91.4(1)	90.7(2)
O1−Cu1−N2	159.9 (4)	160.9(1)	161.8(2)
O101−Cu1−O202	106.2(3)	108.0(1)	108.3(2)
O101−Cu1−N1	164.3(4)	163.5(1)	162.2(2)
O101−Cu1−N2	91.2(4)	89.8(1)	89.4(2)
O202−Cu1−N1	88.4(4)	87.6(1)	89.0(2)
O202−Cu1−N2	100.9(4)	102.4(1)	105.7(2)
N1−Cu1−N2	80.4(4)	81.3(1)	81.8(3)
O2−Cu2−O102	97.2(3)	97.0(1)	95.4(2)
O2−Cu2−O201	92.6(3)	94.2(1)	92.6(2)
O2−Cu2−N3	93.6(3)	90.0(1)	91.2(2)
O2−Cu2−N4	158.2(4)	163.2(1)	163.1(2)
O102−Cu2−O201	106.5(3)	101.3(1)	102.3(2)
O102−Cu2−N3	85.8(3)	92.8(1)	93.9(2)
O102−Cu2−N4	103.0(4)	97.8(1)	100.2(2)
O201−Cu2−N3	165.5(4)	164.7(1)	162.9(2)
O201−Cu2−N4	89.6(4)	90.6(1)	90.5(2)
N3−Cu2−N4	79.9(4)	81.5(1)	81.2(2)
O1−P1−O2	121.7(5)	121.0(2)	122.8(3)
τ (Cu1)	0.07	0.04	0.01
τ (Cu2)	0.12	0.03	0.00

[a] Estimated standard deviations are given in parentheses. Atom labels are shown in Figure 5.

structure is the first example for introduction of a phosphate ester onto a carboxylate-bridged dicopper(II) center. Moreover, for other metal ions, the (μ-phosphate)bis(μ-carboxylato)dimetal structures have barely been established by using the XDK ligand in [ZnM(μ-η^1,η^1-$(PhO)_2PO_2$)(η^1-$(PhO)_2PO_2$)(XDK)$(CH_3OH)_2(H_2O)$] (M = Zn (**16**), Co (**17**)),[12g] [Ca_2(μ-η^1,η^1-$(PhO)_2PO_2$)(η^1-$(PhO)_2PO_2$)(XDK)$(CH_3OH)_3(H_2O)$] (**18**),[12h] [Mg_2(μ-η^1,η^1-$(PhO)_2PO_2$)(η^1-$(PhO)_2PO_2$)(XDK)$(CH_3OH)_3(H_2O)$] (**19a**),[12h] and [Mg_2(μ-η^1,η^1-$(PhO)_2PO_2$)(NO_3)(XDK)$(CH_3OH)_3(H_2O)$] (**19b**).[12h] The Cu···Cu separation of **12** is 4.2685(8) Å, which is significantly longer than those of **16** (3.869(2) Å) and **17** (3.846(1) Å) and slightly longer compared to those of **19a** (4.108(3) Å) and **b** (4.240(5) Å). The appreciable elongation might have resulted from the asymmetrical bridging mode of the biscarboxylate units. One carboxylate oxygen attaches to the Cu atom at the apical site (Cu1−O202 = 2.164(3) Å, Cu2−O102 = 2.182(3) Å), and the other oxygen coordinates to the next Cu center at the basal site (Cu1−O101 = 1.942(3) Å, Cu2−O201 = 1.921(3) Å), resulting in a considerable distortion from a symmetrical syn−syn bidentate bridging structure (Cu1−O202−C201 = 154.6(3)°, Cu1−O101−

(28) (a) Williams, N. H.; Takasaki, B.; Wall, M.; Chin, J. *Acc. Chem. Res.* **1999**, *32*, 485. (b) Wall, M.; Hynes, R. C.; Chin, J. *Angew. Chem., Int. Ed. Engl.* **1993**, *32*, 1633. (c) Young, M. J.; Chin, J. *J. Am. Chem. Soc.* **1995**, *117*, 10577.
(29) (a) Mahroof-Tahir, M.; Karlin, K. D.; Chen, Q.; Zubieta, J. *Inorg. Chim. Acta* **1993**, *207*, 135. (b) Yamaguchi, K.; Akagi, F.; Fujinami, S.; Suzuki, M.; Shionoya, M.; Suzuki, S. *Chem. Commun.* **2001**, 375. (c) Gajda, T.; Kramer, R.; Jancso, A. *Eur. J. Inorg. Chem.* **2000**, 1635. (d) Gajda, T.; Jancso, A.; Mikkola, S.; Lonnberg, H.; Sirges, H. *J. Chem. Soc., Dalton Trans.* **2002**, 1757.
(30) He, C.; Lippard, S. J. *J. Am. Chem. Soc.* **2000**, *122*, 184.
(31) Barker, J. E.; Liu, Y.; Martin, N. D.; Ren, T. *J. Am. Chem. Soc.* **2003**, *125*, 13332.
(32) Raidt, M.; Neuburger, M.; Kaden, T. A. *J. Chem. Soc., Dalton Trans.* **2003**, 1292.

Chart 2

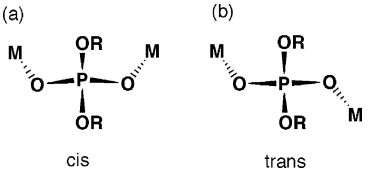

C101 = 125.1(3)°, Cu2−O102−C101 = 155.8(3)°, Cu2−O201−C201 = 130.8(3)°). The diphenyl phosphate (DPP) is accommodated between the two copper(II) ions in a symmetrical μ-η^1,η^1-O,O′ bidentate fashion. The endogeneous oxygen atoms of DPP are involved in the basal plane of each metal center with Cu1−O1 = 1.966(3) Å and Cu2−O2 = 1.954(3) Å. The O1−P−O2 angle of 121.0(2)° is largely deformed from normal values for tetrahedral geometry. Usually, in dinuclear complexes containing 1,3-bridged phosphate and phosphinate units, two metal ions are likely located out-of-plane for the PO_2 phosphinyl plane, leading to the cis conformation as depicted in Chart 2a.[12g,12h,28,29] In the present case, however, the two metal ions deviate up and down with respect to the phosphinyl plane depicted as the trans conformation in Chart 2b. The trans conformation of 1,3-bridging phosphate is very rare and is mainly ascribable to the longer dimetal separation than those with cis oriented 1,3-bridging structures. Complexes **11** and **13** involve closely similar structures to that of **12**. The Cu···Cu separation of **13** (4.315(1) Å) is longer by 0.047 Å than the value of **12**, which may result in the larger distortion around the phosphorus atom with O1−P1−O1 = 122.8(3)°. While these structural features of **13** might indicate that the incorporated bridging phosphate ester is somewhat activated by double Lewis acid binding and by the structural deformation of the phosphate group, the BNPP was not hydrolyzed even by treatment with a stoichiometric amount of hydroxide ions. The result should be notably contrasted to the well-known catalytic functions associated with copper(II) ions in phosphoryl transfer reactions.[28a,33] One of the major problems might be the poor solubility of **13** in polar solvents containing water. Nevertheless, the structures of **11**−**13** could provide useful insights into substrate binding and activation on carboxylate-bridged dimetal active centers in the metalloenzymes that promote phosphoryl transfer reactions.

The structures of **14** and **15** were determined by X-ray crystallography to have a centro symmetry and consist of two square-pyramidal copper(II) ions bridged by two phosphate groups, resulting in an eight-membered $[Cu_2P_2O_4]$ macrocycle (Figure 6 and Table 7). Complexes containing similar eight-membered cores have been prepared with phosphate esters and phosphinates,[34] as well as with nucleoside monophosphates.[35] In complex **14**, the 1,3-bridging DPP

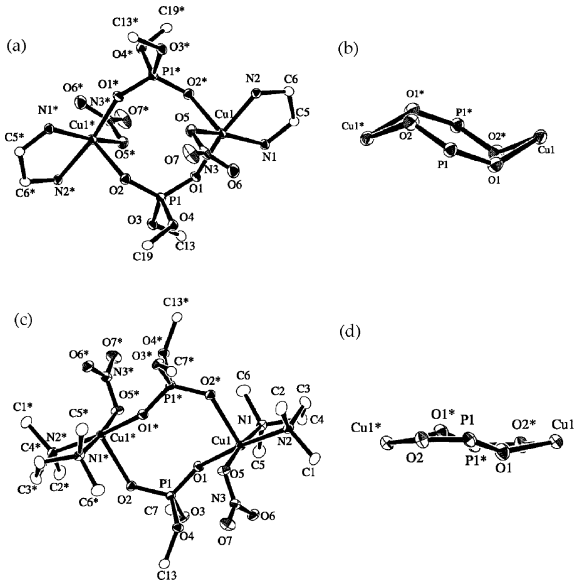

Figure 6. ORTEP plots of (a) **14** and (c) **15** and the $Cu_2P_2O_4$ core structures of (b) **14** and (d) **15**.

Table 7. Selected Bond Distances and Angles for **14** and **15**[a]

	14	**15**
	bond distances (Å)	
Cu1···Cu1*	4.796(1)	5.1191(8)
Cu1−O1	1.931(3)	1.965(1)
Cu1−O2*	2.156(3)	2.239(1)
Cu1−O5	2.019(3)	1.997(1)
Cu1−N1	2.011(3)	2.043(2)
Cu1−N2	2.000(3)	2.063(2)
Cu1···O6	2.667(3)	2.637(1)
	bond angles (deg)	
O1−Cu1−O2*	95.2(1)	94.39(5)
O1−Cu1−O5	93.9(1)	91.65(6)
O1−Cu1−N1	90.7(1)	89.72(6)
O1−Cu1−N2	170.6(1)	172.99(6)
O2*-Cu1−O5	94.4(1)	89.05(5)
O2*-Cu1−N1	105.1(1)	97.43(6)
O2*-Cu1−N2	90.4(1)	92.22(6)
O5−Cu1−N1	159.5(1)	173.26(6)
O5−Cu1−N2	93.2(1)	90.83(6)
N1−Cu1−N2	80.6(1)	87.08(7)
O1−P1−O2	122.9(2)	119.72(8)

[a] Estimated standard deviations are given in parentheses. Atom labels are shown in Figure 6.

connects the two Cu ions in a syn−syn fashion, leading to the $[Cu_2P_2O_4]$ eight-membered puckered ring with a Cu···Cu separation of 4.796(1) Å (Figure 6b). On the other hand, in complex **15**, the bidentate BNPP bridges the two metals is in a syn−anti fashion, and the eight-membered core ring is planar with a longer Cu···Cu distance of 5.1191(8) Å (Figure 6d).

Reactions of Complexes 4 and 6 with Sugar Phosphate Esters. Since the dicarboxylate-bridged dicopper(II) centers with phen-type ligands proved to be a useful platform for binding organic phosphate diesters, as mentioned above, we have tried to introduce sugar phosphates and their analogous

(33) (a) Molenveld, P.; Engbersen, F. J.; Reinhoudt, D. N. *Chem. Soc. Rev.* **2000**, *29*, 75. (b) Hendry, P.; Sargeson, A. M. *Progress in Inorganic Chemistry: Bioinorganic Chemistry*; Lippard, S. J., Ed.; Wiley: New York, 1990; Vol. 38, p 201. (c) Breslow, R.; Huang, D.-L.; Anslyn, E. *Proc. Natl. Acad. Sci. U.S.A.* **1989**, *86*, 1746. (d) Sigman, D. S. *Acc. Chem. Res.* **1986**, *19*, 180.

(34) (a) Deschamps, J. R.; Hartshorn, C. M.; Chang, E. L. *Acta Crystallogr. E* **2002**, *58*, m606. (b) Koga, K.; Ohtsubo, M.; Yamada, Y.; Koikawa, M.; Tokii, T. *Chem. Lett.* **2004**, *33*, 1606.

(35) For example, see: (a) Aoki, K. *J. Am. Chem. Soc.* **1978**, *100*, 7106. (b) Fischer, B. E.; Bau, R. *Inorg. Chem.* **1978**, *17*, 27. (c) Cini, R.; Giorgi, G. *Inorg. Chim. Acta* **1987**, *137*, 87. (d) Giorgi, G.; Cini, R. *Inorg. Chim. Acta* **1988**, *151*, 153. (e) Kovari, E.; Kramer, R. *J. Am. Chem. Soc.* **1996**, *118*, 12704.

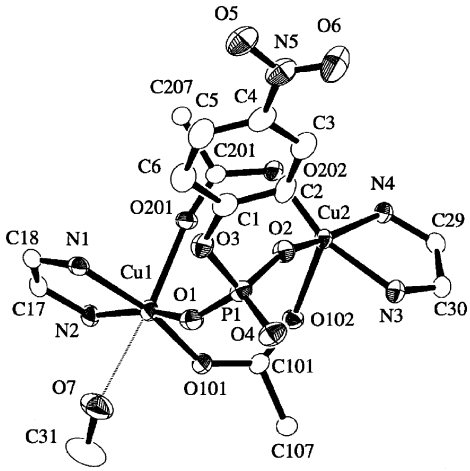

Figure 7. The dicopper(II) core structures of **20**. Most of the XDK and phen are omitted for clarity.

Chart 3

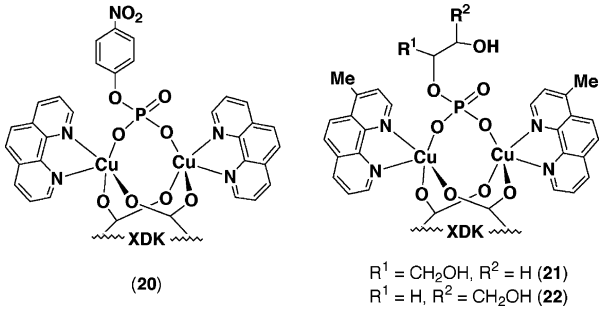

monophosphates onto the dimetal centers using complexes **4** and **6** as starting materials. At first, the reaction of **4** with 4-nitrophenyl phosphate disodium salt, Na_2MNPP, and those of **6** with glycerol 2-phosphate disodium salt, Na_2[Gly-2-**P**], and racemic glycerol 3-phosphate disodium salt, Na_2-[Gly-3-**P**], produced pale blue crystaline complexes, [Cu_2(μ-MNPP)(XDK)(phen)$_2$(CH_3OH)] (**20**) and [Cu_2(μ-Gly-*n*-**P**)(XDK)(Mephen)$_2$] (*n* = 2 (**21**), 3 (**22**)), respectively (Chart 3). The structure of **20** was confirmed by X-ray crystallography to be essentially similar to that of **12** (Figure 7). The two copper ions are bridged by two carboxylate groups of XDK and a phosphate of MNPP dianion, and each end of the dinuclear unit is terminated by a phen ligand, resulting in [N_2O_3] square pyramidal geometry. A solvent methanol is weakly bound to the Cu1 atom (Cu1−O7 = 2.659(3) Å), which is recognized as a semi-coordination resulting from Jahn−Teller distortion. The phosphate group of the MNPP dianion bridges the two metal centers in a μ-1,3-O,O′ mode. The Cu···Cu separation of **20** (4.1825(8) Å) is appreciably shorter than those with the organophosphate diesters **11**−**13** (4.268(3)−4.315(1) Å), which is mainly attributed to the shorter Cu−O(phosphate) bonds (av 1.930 Å) and the smaller O−P−O bridging angle (116.5(1)°). Similar Cu···Cu separations were observed in the tri- and hexanuclear copper(II) complexes with $PhOPO_3^{2-}$ dianions.[36] Recently, Ren et al. have reported the dicopper complex [Cu_2(μ-Gly-2-**P**)$_2$([18]-

Scheme 2

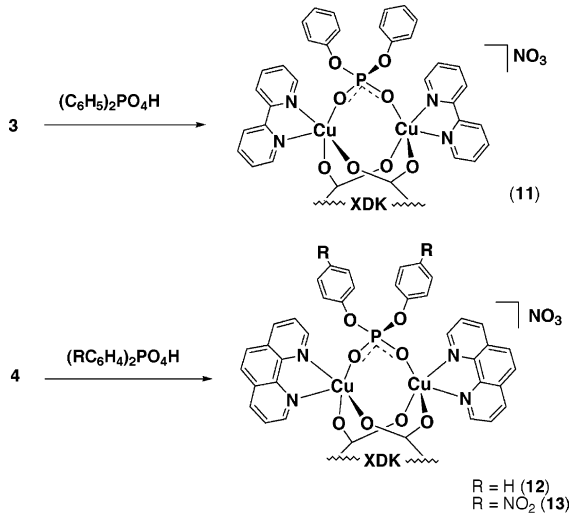

ane-N_6)] ([18]ane-N_6 = 1,4,7,10,13,16-hexaazacyclooctadecane),[31] which is the first characterized transition metal complex of glycerol 2-phosphate and involves two monoatom-bridging phosphate esters in a η^1,η^1-O fashion. In complexes **21** and **22**, however, the glycerol phosphate ester is estimated to act as a 1,3-O,O′-bridging ligand, in the light of the crystal structure of **20** and **27a** and the spectral similarity to **20**. The binding constants (apparent association constants)[31] of **4** toward phosphate monoester dianions were determined from the visible absorption spectral changes in methanol or methanol/water solutions, and the values for $MNPP^{2-}$ (1.1×10^4) and Gly-2-$\mathbf{P}^{2-}$ (1.0×10^4) were about 10× larger than that for the DPP phosphodiester monoanion (0.96×10^3).

Reactions of complexes **4** and **6** with Na_2[α-D-Glc-1-**P**], Na_2[D-Glc-6-**P**], Na_2[D-Man-6-**P**], Na_2[D-Fru-6-**P**], and Na_n-[D-Fru-1,6-$\mathbf{P}_2$] in a methanol/water mixed solvent yielded a series of dicopper(II) sugar−phosphate complexes, [Cu_2(μ-Sugar-**P**)(XDK)(L)$_2$] (L = phen, Sugar-**P** = α-D-Glc-1-**P** (**23a**), D-Glc-6-**P** (**24a**), D-Man-6-**P** (**25a**), D-Fru-6-**P** (**26a**); L = Mephen, Sugar-**P** = α-D-Glc-1-**P** (**23b**), D-Glc-6-**P** (**24b**), D-Fru-6-**P** (**26b**)), and the tetracopper(II) complexes of [Cu_4(μ-D-Fru-1,6-$\mathbf{P}_2$)(XDK)$_2$(L)$_4$] (L = phen (**27a**), Mephen (**27b**)) (Schemes 3 and 4). The IR spectra of **23**−**27** closely resembled those of the glycerol phosphate complexes **21** and **22** except for the somewhat broad peaks around 1100 cm^{-1}, characteristic of sugar residues. The ESI mass spectra for methanolic solutions of **23**−**26** exhibited the monocationic parent peaks corresponding to {[Cu_2(Sugar-**P**)(XDK)(L)$_2$]+H}$^+$; the distributions of the isotopomers were also in agreement with the complex formula (Figure S15). In the UV spectra of **23**−**27**, a broad band appeared in the range of 710−720 nm, corresponding to d−d transitions of Cu(II) ions, and in the circular dichroism (CD) spectra, appreciable Cotton effects were observed in the range of 600−800 nm (Figure 8). These spectral data suggested that the chiral sugar phosphate esters were incorporated into the dinuclear copper(II) centers bridged by the XDK ligand. The intensities of the CD spectra for **23**−**27** were at least

(36) (a) Fry, F. H.; Jensen, P.; Kepert, C. M.; Spiccia, L. *Inorg. Chem.* **2003**, *42*, 5637. (b) Itoh, M.; Nakazawa, J.; Maeda, K.; Kano, K.; Mizutani, T.; Kodera, M. *Inorg. Chem.* **2005**, *44*, 691.

Scheme 3

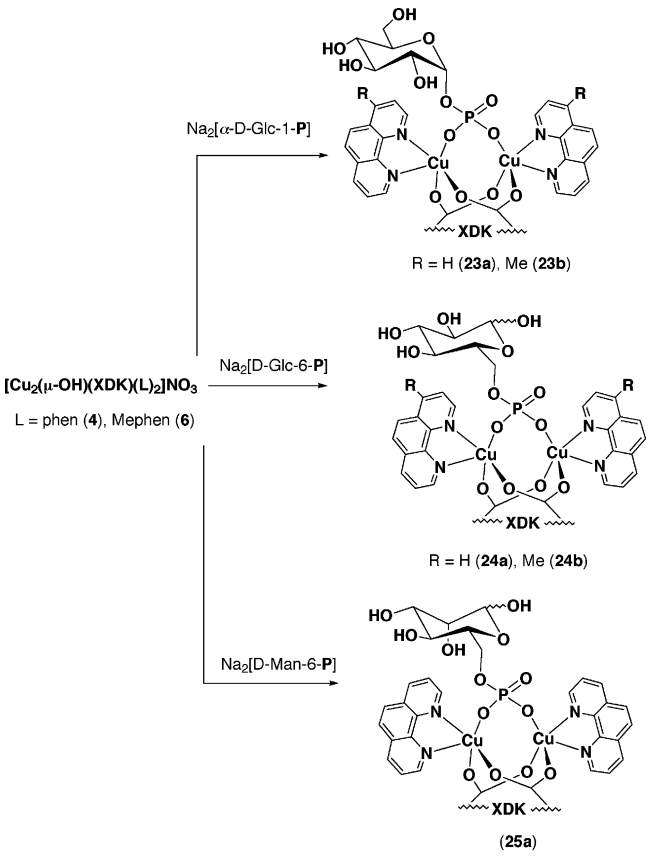

Scheme 4

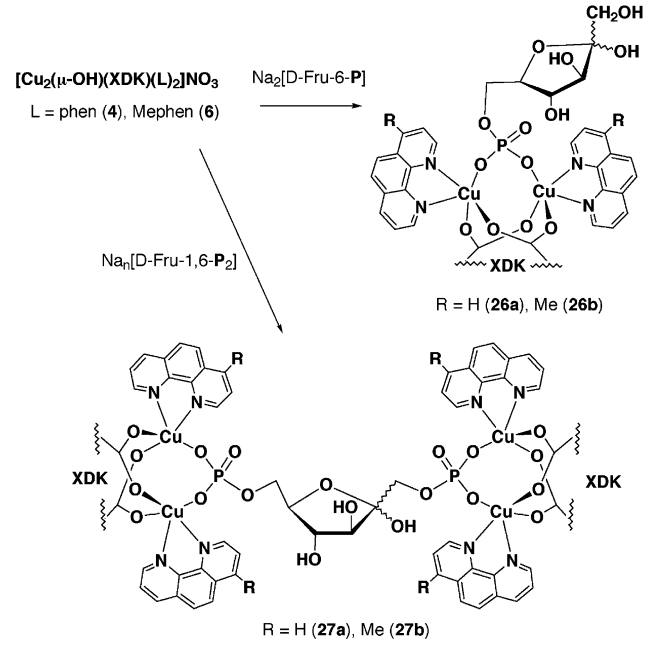

10-fold weaker than that of $[Cu_3\{\mu\text{-(D-Glc)}_2\text{-tacn}\}_2(XDK)]$ ((D-Glc)$_2$-tacn = N,N′-bis(β-D-glucopyranosyl)-1,4,7-triazacyclononane),[13] where the *N*-β-D-glucopyranoside bridges two copper(II) ions through the C2 and C3 hydroxyl groups as well as the glycosidic nitrogen atoms, the sugar hydroxyl groups directly coordinating to the metal centers. It is assumed that, in the present complexes, the sugar phosphate esters are bound to the dimetal centers only by the phosphate group, and the chiral sugar moieties are away from the copper ions, on the basis of the weak CD spectra as well as the X-ray structures of **20** and **27a**. For complexes **24**−**27**, two anomeric forms of the carbohydrate residue and two enantiomeric $\{Cu_2(XDK)(L)_2\}$ structures with respect to its pseudo-C_2 symmetry are estimated to be involved, which may lead to a complicated distribution of diastereomers and, thus, result in delicate dependency of the CD spectral patters on the sugar units.

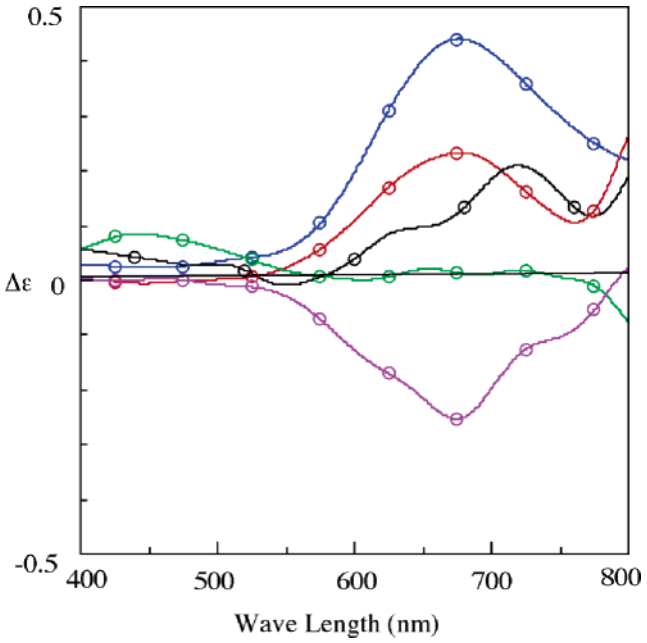

Figure 8. Circular dichroism spectra for **23a** (red), **24a** (blue), **25a** (black), **26a** (green), and **27a** (violet) in DMF.

Structure of Tetranuclear Cu(II) Complex Containing D-Fructose 1,6-bisphosphate (27a). The detailed structure of **27a** was determined by X-ray crystallography (Figures 9 and 10; Table 8). The asymmetric unit contains two neutral tetranuclear copper(II) complexes formulated as $[Cu_4(\mu\text{-D-Fru-1,6-}\mathbf{P}_2)(XDK)_2(phen)_4]$, which are not chemically identical to each other. One involves an α-anomer of D-fructose 1,6-bisphosphate ($[Cu_4(\mu\text{-α-D-Fru-1,6-}\mathbf{P}_2)(XDK)_2(phen)_4]$ indicated as Mol **A** in Figure 9) and the other has a β-anomer of the bisphosphate ($[Cu_4(\mu\text{-}\beta\text{-D-Fru-1,6-}\mathbf{P}_2)(XDK)_2(phen)_4]$ indicated as Mol **B** in Figure 10). The two complex molecules are weakly interacted through $\pi-\pi$ stacking between the phen ligands. In each molecule, the two phosphate groups of D-Fru-1,6-$\mathbf{P}_2$ are bound in a bidentate 1,3-O,O′-bridging mode to the biscarboxylate-bridged dicopper(II) units, $\{Cu_2(XDK)(phen)_2\}^{2+}$. The structures are essentially similar to those observed in complexes **12**, **13**, and **20**, consisting of two square-pyramidal $[N_2O_3]$ copper(II) ions asymmetrically bridged by two carboxylate groups of XDK in a pseudo-C_2 symmetrical fashion.

The tetranuclear core structure of $[Cu_4(\mu\text{-α-D-Fru-1,6-}\mathbf{P}_2)(XDK)_2(phen)_4]$ (Mol **A**) is illustrated in Figure 9. The two phsophate groups at the C1 and C6 positions of the α-D-Fru-1,6-$\mathbf{P}_2$ tetraanion bridge the two dicopper(II) units in a syn−syn bidentate mode with a trans conformation. The two

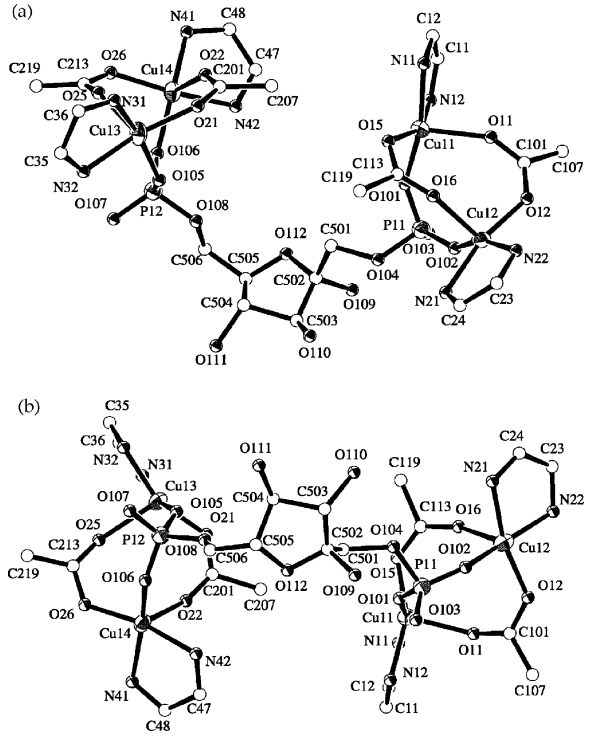

Figure 9. (a) ORTEP plot for the core structure of [Cu_4(μ-α-D-Fru-1,6-$\mathbf{P}_2$)(XDK)$_2$(phen)$_4$] (Mol **A**) in **27a** and (b) that viewed vertical to the franoside ring. The O, N, and C atoms are drawn with arbitrary spheres.

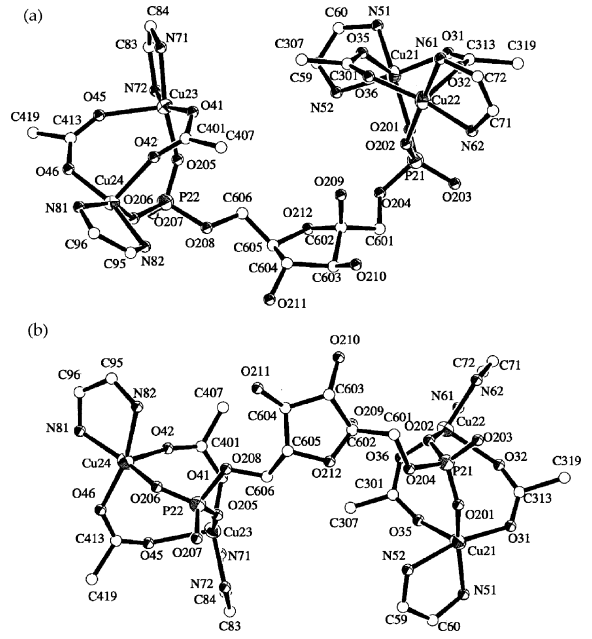

Figure 10. (a) ORTEP plot for the core structure of [Cu_4(μ-β-D-Fru-1,6-$\mathbf{P}_2$)(XDK)$_2$(phen)$_4$] (Mol **B**) in **27a** and (b) that viewed vertical to the franoside ring. The O, N, and C atoms are drawn with arbitrary spheres.

triply bridged dicopper(II) fragments, {Cu_2(μ-PO_4)(XDK)-(phen)$_2$}, are nearly enantiomeric with Cu11···Cu12 = 4.100(2) Å and Cu13···Cu14 = 4.047(2) Å. The P11···P12 separation is 8.189(6) Å, and the two dicopper units are located in the same side with respect to the furanose ring. The average bond distance between the phosphate oxygen and the copper atoms is 1.923 Å which is somewhat shorter than the values of **12** (av 1.960 Å) and **13** (av 1.977 Å), indicating stronger affinity of the phosphate monoester dianions to dicopper(II) unit compared to that of the phosphate diester monoanions. The average O−P−O angle

Table 8. Selected Bond Distances and Angles for **27a**[a]

Mol **A**		Mol **B**	
bond distances (Å)			
Cu11···Cu12	4.100(2)	Cu21···Cu22	4.042(2)
Cu13···Cu14	4.047(2)	Cu23···Cu24	4.096(2)
P11···P12	8.189(6)	P21···P22	8.458(6)
Cu11−O11	2.140(9)	Cu21−O31	1.953(8)
Cu11−O15	2.000(7)	Cu21−O35	2.218(7)
Cu11−O101	1.890(7)	Cu21−O201	1.915(8)
Cu11−N11	2.06(1)	Cu21−N51	1.997(9)
Cu11−N12	2.089(8)	Cu21−N52	2.07(1)
Cu12−O12	1.954(7)	Cu22−O32	2.187(8)
Cu12−O16	2.213(9)	Cu22−O36	1.965(8)
Cu12−O102	1.896(8)	Cu22−O202	1.892(9)
Cu12−N21	2.07(1)	Cu22−N61	2.08(1)
Cu12−N22	1.98(1)	Cu22−N62	2.05(1)
Cu13−O21	1.967(9)	Cu23−O41	1.930(8)
Cu13−O25	2.176(8)	Cu23−O45	2.203(8)
Cu13−O105	1.984(8)	Cu23−O205	1.907(9)
Cu13−N31	1.98(1)	Cu23−N71	1.983(9)
Cu13−N32	2.06(1)	Cu23−N72	2.054(9)
Cu14−O22	2.214(7)	Cu24−O42	2.209(8)
Cu14−O26	1.961(9)	Cu24−O46	1.952(8)
Cu14−O106	1.920(8)	Cu24−O206	1.943(7)
Cu14−N41	2.036(9)	Cu24−N81	2.042(9)
Cu14−N42	2.04(1)	Cu24−N82	2.055(9)
bond angles (deg)			
O11−Cu11−O15	111.6(3)	O31−Cu21−O35	102.4(3)
O11−Cu11−O101	100.0(3)	O31−Cu21−O201	94.1(4)
O11−Cu11−N11	91.9(4)	O31−Cu21−N51	90.3(4)
O11−Cu11−N12	89.7(3)	O31−Cu21−N52	167.4(3)
O15−Cu11−O101	95.2(3)	O35−Cu21−O201	110.5(3)
O15−Cu11−N11	88.7(4)	O35−Cu21−N51	91.6(3)
O15−Cu11−N12	156.2(4)	O35−Cu21−N52	85.9(3)
O101−Cu11−N11	165.0(4)	O201−Cu21−N51	155.8(3)
O101−Cu11−N12	91.0(3)	O201−Cu21−N52	91.7(4)
N11−Cu11−N12	79.9(4)	N51−Cu21−N52	79.9(4)
O12−Cu12−O16	102.7(3)	O32−Cu22−O36	109.8(3)
O12−Cu12−O102	95.2(3)	O32−Cu22−O202	99.3(3)
O12−Cu12−N21	166.6(4)	O32−Cu22−N61	89.3(3)
O12−Cu12−N22	90.2(4)	O32−Cu22−N62	92.6(4)
O16−Cu12−O102	102.0(4)	O36−Cu22−O202	94.0(4)
O16−Cu12−N21	87.3(4)	O36−Cu22−N61	87.2(4)
O16−Cu12−N22	94.0(4)	O36−Cu22−N62	155.3(4)
O102−Cu12−N21	91.4(4)	O202−Cu22−N61	170.2(3)
O102−Cu12−N22	161.6(4)	O202−Cu22−N62	92.4(4)
N21−Cu12−N22	80.1(4)	N61−Cu22−N62	82.7(4)
O21−Cu13−O25	108.3(3)	O41−Cu23−O45	109.3(3)
O21−Cu13−O105	94.7(4)	O41−Cu23−O205	94.9(4)
O21−Cu13−N31	92.0(4)	O41−Cu23−N71	91.3(3)
O21−Cu13−N32	157.4(4)	O41−Cu23−N72	158.5(4)
O25−Cu13−O105	101.4(3)	O45−Cu23−O205	98.2(4)
O25−Cu13−N31	88.6(4)	O45−Cu23−N71	92.2(3)
O25−Cu13−N32	91.8(4)	O45−Cu23−N72	91.0(4)
O105−Cu13−N31	165.6(4)	O205−Cu23−N71	165.3(4)
O105−Cu13−N32	91.0(4)	O205−Cu23−N72	88.7(4)
N31−Cu13−N32	78.2(5)	N71−Cu23−N72	80.8(4)
O22−Cu14−O26	102.9(3)	O42−Cu24−O46	101.4(3)
O22−Cu14−O106	107.0(3)	O42−Cu24−O206	105.7(3)
O22−Cu14−N41	93.2(3)	O42−Cu24−N81	94.2(3)
O22−Cu14−N42	85.5(3)	O42−Cu24−N82	89.1(4)
O26−Cu14−O106	93.7(4)	O46−Cu24−O206	95.1(3)
O26−Cu14−N41	89.5 (4)	O46−Cu24−N81	88.3(3)
O26−Cu14−N42	168.3(3)	O46−Cu24−N82	165.5(4)
O106−Cu14−N41	158.2(3)	O206−Cu24−N81	158.7(4)
O106−Cu14−N42	91.4(4)	O206−Cu24−N82	91.7(3)
N41−Cu14−N42	82.0(4)	N81−Cu24−N82	80.7(4)
O101−P11−O102	114.6(5)	O201−P21−O202	113.5(5)
O105−P12−O106	116.2(5)	O205−P22−O206	117.3(5)

[a] Estimated standard deviations are given in parentheses. Atom labels are shown in Figures 9 and 10. Mol **A** is [Cu_4(α-D-Fru-1,6-$\mathbf{P}_2$)(XDK)$_2$(phen)$_4$], and Mol **B** is [Cu_4(β-D-Fru-1,6-$\mathbf{P}_2$)(XDK)$_2$(phen)$_4$].

for the bidentate phosphate groups is 115.4°, indicating smaller deformation of the tetrahedral phosphorus atoms compared to those in the phosphate diester complexes **12** and **13**. The five-membered furanose ring adopts an envelop conformation with the C3 carbon at an apex position (^{3}E), which might be stabilized by the unique hydrogen-bonding interaction around the C1 phosphate group. On the basis of interatomic distances, a strong hydrogen-bonding interaction may exist between the α-anomeric C2 hydroxyl group and the C1 phosphate oxygen atom (O109···O104 = 2.68(1) Å), and in addition, the C2 hydroxyl group forms a weak hydrogen bond with the exogeneous phosphate oxygen atom (O109···O103 = 2.93(2) Å). In contrast, no hydrogen bonding interaction exists around the C6 phosphate group. The structure of [Cu_4(μ-β-D-Fru-1,6-**P**$_2$)(XDK)$_2$(phen)$_4$] (Mol **B**) has a tetranuclear core similar to that of Mol **A**, in which a β-D-fructose 1,6-bisphosphate bridges two {Cu_2(XDK)(phen)$_2$}$^{2+}$ units (Cu21···Cu22 = 4.042(2) Å, Cu23···Cu24 = 4.096(2) Å) (Figure 10). The two phosphate groups are located on the same side with respect to the sugar ring, and the P21 and P22 atoms are 8.458(6) Å apart, 0.27 Å longer than that observed in Mol **A**. Each phosphate takes the 1,3-O,O′-bridging structure with a trans conformation, like in Mol **A**, with the similar structural parameters of av P−O = 1.914 Å and av O−P−O = 115.4°. The furanose ring adopts an envelop conformation (E_2) where the C2 carbon deviates toward the exo direction with respect to the C6 branch. The characteristic hydrogen bondings are also observed around the C1 phosphate group, the β-anomeric C2 hydroxyl group forming bifurcated hydrogen bonds with the C1 phosphate oxygen (O209···O204 = 2.79(1) Å), the bridging phosphate oxygen (O209···O202 = 2.83(1) Å), and the C3 hydroxyl group (O209···O210 = 2.67(1) Å). The hydrogen-bonding networks around the C1 phosphate group observed in both Mol **A** and **B** may result in rigid orientation of the sugar moiety with respect to the phosphate-bridged dicopper fragment. The conformations around the C1−C2 and C1−O1 single bonds in Mol **A** and **B** are essentially similar as indicated by the torsion angles of C104−C501−C502−C109 = −40(1)° and P11−O104−C501−C502 = 112(1)° for Mol **A** and O204−C601−C602−O209 = −62.6(9)° and P21−O204−C601−C602 = 114.1(8)° for Mol **B**. There is no appreciable intramolecular hydrogen-bonding interaction around the C6 phosphate group in Mol **B**, just like in Mol **A**, which may allow free rotation of C5−C6 and C6−O6 single bonds and result in the different orientation of the C6 phosphate group in comparison with that in Mol **A**; the torsion angles are P12−O108−C506−C505 = −170(1)° and O112−C505−C506−O108 = −59(1)° for Mol **A** and P22−O208−C606−C605 = −160.0(9)° and O212−C605−C606−O208 = 178.1(9)° for Mol **B**.

Comparison of the Structures of 27a and Fructose-1,6-bisphosphatase. It should be of significant importance to compare the structure of α-D-fructose 1,6-bisphosphate in complex **27a** to the active site of fructose-1,6-bisphosphatase complexed with the substrate analogue.[5a] Fructose-1,6-bisphosphatase (Fru-1,6-Pase) plays a critical role in regulating the gluconeogenesis pathway and promotes hydrolysis

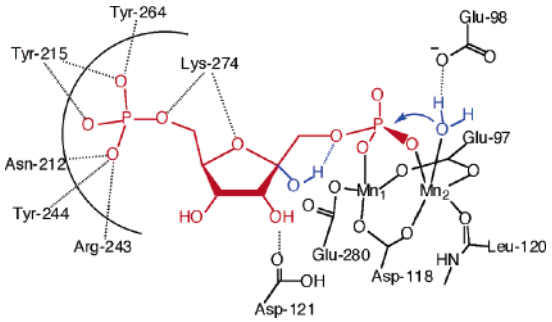

Figure 11. Schematic depiction of the structure of the active site of Fru-1,6-Pase complexed with Mn^{2+} ions and the substrate-analogous inhibitor AhG-1,6-**P**$_2$.[5a] The AhG-1,6-**P**$_2$ unit is drawn in red, and the postulated mechanistic requirements are blue.[5a]

of D-Fru-1,6-**P**$_2$ to D-Fru-6-**P**. The C1 phsophate ester bond of α-D-Fru-1,6-**P**$_2$ is specifically cleaved in the presence of divalent metal ions, such as Mg^{2+}, Mn^{2+}, and Zn^{2+}. A plausible mechanism has been proposed in light of the kinetic studies as well as the X-ray crystal structure for Fru-1,6-Pase complexed with Mn^{2+} (or Zn^{2+}) ions and 2,5-anhydro-D-glucitol-1,6-bisphosphate (AhG-1,6,-**P**$_2$) which is a substrate analogue to α-D-Fru-1,6-**P**$_2$ but bearing no hydroxyl group at the C2 position (Figures 11 and 12a).[5a] From model building based on the structure of the Fru-1,6-Pase/Mn^{2+}/AhG-1,6-**P**$_2$ complex, a plausible catalytic mechanism was proposed as follows:[5a] (1) The phosphate group is activated by binding to the two Lewis acidic metal ions, as well as by the postulated hydrogen bond between the C2 hydroxyl group and the C1 phosphate oxygen atoms. (2) A water molecule is activated by binding to the Mn2 ions with the help of a hydrogen-bonding interaction with the carboxylate group of Glu-98. (3) The in-line nucleophilic attack occurs at the C1 phosphate group from the opposite direction to the phosphate ester oxygen atom. The features postulated with the true substrate α-D-Fru-1,6-**P**$_2$ are superimposed as the blue-colored parts on the schematic structure with AhG-1,6-**P**$_2$ (drawn in red) in Figure 11. The structure for the part of α-D-Fru-1,6-**P**$_2$ in **27a** (Mol **A**) is illustrated in Figure 12b. The conformation of the furanose ring of α-D-Fru-1,6-**P**$_2$ in Mol **A** is quite similar to that of AhG-1,6-**P**$_2$ in the enzyme (Figure 12a), and the orientation of the C1 phosphate arms also resemble each other. The strong hydrogen-bonding interaction between the C2 hydroxyl group (O2) and the C1 phosphate oxygen (O1) is definitively observed (O1···O2 = 2.68(1) Å) in the Cu_2/α-D-Fru-1,6-**P**$_2$ structure, which strongly supports the corresponding intramolecular hydrogen bond postulated in the catalytic mechanism mentioned above. The short interatomic distance, O2···O_γ = 2.93(2) Å, also suggested that a polar interaction between the C2 hydroxyl group and the bridging phsophate oxygen (O_γ) might be involved in the mechanism. In Mol **B** with β-D-Fru-1,6-**P**$_2$, the hydrogen bond between the C2 hydroxyl group and the C1 phosphate oxygen (O1···O2 = 2.79(1) Å) is not as strong as the one (2.68(1) Å) in the α-D-Fru-1,6-**P**$_2$ unit of Mol **A**, which is mainly attributable to the presence of a hydrogen bond between the cis-oriented C2 and C3 hydroxyl groups (O2···O3 = 2.67(1) Å) (Figure 12c). The positions of dimetal ions with respect to the C1 phosphate group in Mol **A** and

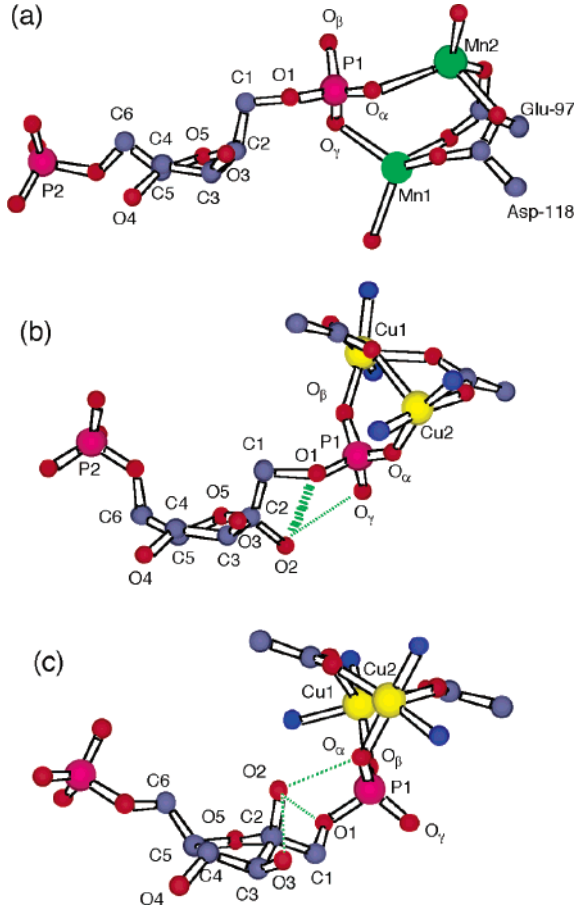

Figure 12. (a) Perspective drawing for the AhG-1,6-$\mathbf{P}_2$ unit with its C1 phosphate group bound to the Mn^{2+} ions in the active site of Fru-1,6-Pase.[5a] (b) Perspective drawing for the α-D-Fru-1,6-$\mathbf{P}_2$ unit with its C1 phosphate bound to the Cu^{2+} ions in Mol **A** of **27a**. (c) Perspective drawing for the β-D-Fru-1,6-$\mathbf{P}_2$ unit with its C1 phosphate bound to the Cu^{2+} ions in Mol **B** of **27a**. Mn (green), Cu (yellow), P (violet), O (red), N (blue), and C (gray). The systematic atomic numbering scheme is adopted to compare the structures to each other.

B are largely different from those in the enzyme active site, in which the coordination sites, favorable to in-line nucleophilic attack to the phosphate unit, are rigidly occupied by phen and XDK ligands (Figures 12b and c). These features may be responsible for nonfunctionality of the present model system for hydrolysis of sugar phosphate esters.

Conclusion

The dicarboxylate ligand XDK has been proven to stabilize a series of (μ-hydroxo)bis(μ-carboxylato)dicopper(II) complexes with N-donor auxiliary chelating ligands, $[Cu_2(\mu\text{-OH})(XDK)(L)_2]^+$ (L = tetmen, tmen, bpy, Me_2bpy, phen, and Mephen). Among them, the complexes with phen and Mephen ligands (**4** and **6**) have been elucidated as providing effective carboxylate-bridged dicopper scaffolds suitable for the fixing of organic phosphate esters and sugar phosphates. In particular, the tetranuclear copper(II) complex with D-fructose 1,6-bisphosphate, $[Cu_4(\mu\text{-D-Fru-1,6-}\mathbf{P}_2)(XDK)_2(phen)_4]$ (**27a**), was characterized by X-ray crystallography to consist of two biscarboxylate-bridged dicopper(II) fragments connected by an α- or β-anomer of D-Fru-1,6-$\mathbf{P}_2$, resulting in a 1:1 mixture of $[Cu_4(\mu\text{-}\alpha\text{-D-Fru-1,6-}\mathbf{P}_2)(XDK)_2(phen)_4]$ and $[Cu_4(\mu\text{-}\beta\text{-D-Fru-1,6-}\mathbf{P}_2)(XDK)_2(phen)_4]$. In the structure with α-D-Fru-1,6-$\mathbf{P}_2$, the C2 hydroxyl group forms a strong hydrogen bond with the C1 phosphate oxygen atom, and the orientation of the sugar moiety with respect to the C1 phosphate group is fixed by the characteristic hydrogen-bonding interaction around the C2 hydroxyl group. These structural features of **27a** could provide useful information as a substrate binding model for fructose-1,6-bisphosphatase.

Acknowledgment. The authors are grateful to Professor Stephen. J. Lippard of Massachusetts Institute of Technology for valuable discussion and comments. This work was partly supported by Grant-in-Aid for Scientific Research from the Ministry of Education, Culture, Sports, Science, and Technology of Japan.

Supporting Information Available: X-ray crystallographic files in CIF format, ORTEP plots of complexes **1**−**6**, **11**−**15**, **20**, and **27a**, and ESI mass spectra of **23a**, **b**, **24a**, **b**, **25a**, **26a**, and **b**. This material is available free of charge via the Internet at http://pubs.acs.org.

IC051942D